BER Analysis for OTFS Zero Forcing Receiver

Prem Singh, Khushboo Yadav, Himanshu B. Mishra, *Member, IEEE*, and Rohit Budhiraja

***Abstract*— We derive closed form bit error rate (BER) expression for orthogonal time frequency space (OTFS) zero-forcing (ZF) receiver with perfect and imperfect receive channel information. Depending on the delay-Doppler locations of the propagation paths of the OTFS channel $\mathbf{H}$, the expression $\mathbf{H}^H\mathbf{H}$ is shown to have either distinct or repetitive eigenvalues. When $\mathbf{H}^H\mathbf{H}$ has two or less distinct eigenvalues and the remaining ones are repetitive, we derive the probability distribution function (pdf) of the signal-to-noise-plus-interference-ratio (SINR) of the ZF receiver. A closed form BER expression is then derived by averaging the conditional BER over the SINR pdf. When $\mathbf{H}^H\mathbf{H}$ has n distinct eigenvalues, we use numerical integration to derive a generalized expression for the SINR pdf. We show that this pdf can be tightly approximated by the Gamma pdf, and then use it to derive the BER expression. The derived OTFS ZF BER expression therefore, unlike the existing ones in the literature, does not require averaging over multiple channel realizations. We show, for different modulation schemes and OTFS system parameters, that the BER calculated using the derived expressions closely matches the one calculated numerically.**

***Index Terms*— Bit error rate (BER), orthogonal time-frequency space (OTFS), zero forcing (ZF) receiver.**

I. Introduction

A WIRELESS channel is selective in frequency and time domains due to the multiple propagation delays and Doppler shift [1]. Orthogonal frequency division multiplexing (OFDM) efficiently handles high frequency selectivity and low-to-moderate time selectivity, by first multiplexing the symbols in the time-frequency domain, and then by adding the cyclic prefix to the time domain symbols [1]. A highly time-selective channel, which occurs due to high Doppler shift, however, disturbs the inter-subcarrier orthogonality in OFDM systems. This causes inter-subcarrier interference, which significantly degrades its performance [2]. An orthogonal time frequency space (OTFS) system [3]–[10], in contrast to OFDM, multiplexes symbols in the delay-Doppler domain, where even a highly frequency- and time-selective channel appears as approximately constant. An OTFS system, for vehicular speeds ranging from 30 km/h to 500 km/h, consequently has a significantly lower bit error rate (BER) than the OFDM system [10]. Additionally, the delay-Doppler domain channel is known to be sparse [11], which can also be leveraged to reduce channel estimation and data detection complexity of OTFS systems. Reference [12] provides an excellent overview of the OTFS scheme, and the future research challenges which need to be addressed in OTFS in context of the 6G wireless networks.

Design of OTFS receivers, which can operate at high Doppler shifts, and can exploit the inherent delay-Doppler channel sparsity, has recently attracted research attention [6]–[11], [13]–[20]. The OTFS receivers designs can broadly be classified as non-linear and linear. Non-linear receivers e.g., maximum likelihood (ML) and maximum a posteriori (MAP), have extremely high computational complexity. Surabhi *et al.* in [13] analyzed the diversity of an ML receiver in a single-input single-output (SISO)/multiple-input multiple-output (MIMO)-OTFS system. Reference [14] investigated a message passing (MP)-aided receiver for a SISO-OTFS system with perfect channel state information (CSI). The MP algorithm reduces the receiver complexity, and provides approximate MAP solution by exploiting the delay-Doppler domain channel sparsity. Ge *et al.* in [7] designed a fractionally spaced sampling (FSS) OTFS non-linear receiver wherein the sampling rate is an integer multiple of the symbol rate. This work exploited the delay-Doppler channel sparsity and the channel diversity via FSS to construct two MP based non-linear equalization algorithms for symbol detection. Gaudio *et al.* in [8] developed a soft-output MP detector for an OTFS-aided radar system that exploits the delay-Doppler channel sparsity. References [15] and [16] numerically quantified the MP receiver performance for a phase-noise impaired MIMO-OTFS and mmWave-aided SISO-OTFS system, respectively. Reference [6] developed a non-linear OTFS detector by combining the QR decomposition-aided time-domain equalization and maximum ratio combining. The authors in [10] designed a non-linear receiver for SISO-OTFS systems using sphere decoding (SD), and numerically quantified its block error rate. Murali and Chockalingam in [17] proposed a Markov chain Monte Carlo sampling (MCMCS)-based non-linear

Manuscript received June 22, 2021; revised October 27, 2021 and January 9, 2022; accepted January 24, 2022. Date of publication February 1, 2022; date of current version April 18, 2022. This research was supported by the project (SRG/2019/000861) Science and Engineering Research Board, Department of Science and Technology, Government of India. Rohit Budhiraja would like to gratefully acknowledge the financial assistance received from Ministry of Electronics and Information Technology (MeitY), Govt. of India, under the "Next Generation Wireless Research and Standardization on 5G+ and 6G" Project. An earlier version of this paper was presented in part at the IEEE SPAWC 2021 [DOI: 10.1109/SPAWC51858.2021.9593186]. The associate editor coordinating the review of this article and approving it for publication was S. Jin. *(Corresponding author: Himanshu B. Mishra.)*

Prem Singh is with the Faculty of Networking, Communication and Signal Processing, International Institute of Information Technology (IIIT) Bangalore, Bengaluru 560100, India (e-mail: prem.singh@iiitb.ac.in).

Khushboo Yadav is with Qualcomm, Hyderabad 500081, India (e-mail: khusyada@qti.qualcomm.com).

Himanshu B. Mishra is with the Department of Electronics Engineering, Indian Institute of Technology (Indian School of Mines) Dhanbad, Dhanbad 826004, India (e-mail: himanshu@iitism.ac.in).

Rohit Budhiraja is with the Department of Electrical Engineering, Indian Institute of Technology (IIT) Kanpur, Kanpur 208016, India (e-mail: rohitbr@iitk.ac.in).

Color versions of one or more figures in this article are available at https://doi.org/10.1109/TCOMM.2022.3148363.

Digital Object Identifier 10.1109/TCOMM.2022.3148363

TABLE I
SUMMARY OF LITERATURE FOCUSING ON RECEIVER DESIGN FOR OTFS SYSTEMS

Ref.	Scenario	CSI	Scheme	Nature	Analytical BER
[10], [19]	SISO	Perfect	SD	non-linear	×
[7], [8], [14], [16]	SISO	Perfect	MP	non-linear	×
[9], [11]	SISO	Perfect	ZF, MMSE	linear	×
[18]	2×2 MIMO	Perfect	ZF, MMSE	linear	×
[13], [15]	MIMO	Perfect	ML,MP	non-linear	×
[17]	SISO	Imperfect	MCMCS	non-linear	×
[20] / [25]	MIMO/SISO	Imperfect/Perfect	ZF, MMSE	linear	Instantaneous BER
Proposed	**SISO**	**Perfect, Imperfect**	**ZF**	linear	✔

receiver for SISO-OTFS systems. Reference [19] proposed a reduced-complexity non-linear variational-Bayes-based receiver for SISO-OTFS systems.

The OTFS literature has also investigated linear receivers e.g., zero-forcing (ZF) [11], [20], [21] and minimum mean square error (MMSE) [9], [11], [20], which have much lower complexity than their ML/MP-aided counterparts. Surabhi and Chockalingam in [11] exploited the doubly-circulant structure of the OTFS channel matrix to design reduced-complexity ZF and MMSE receivers for SISO-OTFS systems. Tiwari *et al.* in [9] leveraged the sparsity and quasi-banded structure of matrices involved in the demodulation process, and designed a linear MMSE (LMMSE) receiver with log-linear order of complexity. Reference [18] designed a low-complexity ZF/MMSE receiver for 2×2 MIMO-OTFS systems. The ZF receiver is the simplest low-complexity linear design which, without requiring the noise and channel statistics, provides reasonable BER [11], [20]–[22]. The MMSE receiver, by exploiting the priori knowledge of the noise variance and channel correlations, outperforms the ZF receiver. However, the noise variance and channel correlation knowledge is difficult to acquire in practice. The ZF receivers, due to aforementioned reasons, are widely used in commercial fifth generation cellular systems [23], [24], and are expected to be used in the future generation of wireless systems [23].

The aforementioned non-linear and linear OTFS receiver literature is summarized in Table I. We see that these works have mostly focused on the OTFS receiver design, and has not yet analytically derived their BER. An exception being the BER expression in [20], [25], which is conditioned on the signal-to-noise-plus-interference-ratio (SINR) of MIMO-OTFS ZF and MMSE receivers. This expression, therefore, requires at least $\mathcal{O}(1000)$ channel realizations for averaging the conditional BER to accurately calculate its true value. This expression also computes SINR for each channel realization to calculate BER, which makes it computationally intensive. Reference [25] derived theoretical BER for the weighted-type fractional Fourier transform (WFRFT)-OTFS systems over *static multi-path channels* by considering ZF and MMSE receivers. This work also derived the *instantaneous BER*, which requires averaging over a large number of channel realization to predict the true BER. The current work, in contrast, i) considers a highly time-varying channel; and ii) derives *average BER* by averaging instantaneous BER over the SINR pdf. Before designing any practical communication systems, their performance is investigated by performing extensive system-level numerical simulations in realistic channel conditions [26]. The closed-form BER expressions are commonly used by system designers to abstract the BER in a time-efficient manner as they can be used to get realistic performance without actually transmitting data. This considerably reduces the simulation time. These expressions are, however, beneficial only if they closely mimic the actual performance. This motivates us to derive analytical BER expressions which can achieve this objective. In light of the above observations and the fact that the BER of ZF-OTFS receivers has not yet been rigorously studied in the existing literature motivates the current work whose **key contributions** are listed below in detail. 1) For the OTFS channel matrix $\mathbf{H}$, we show that the matrix $\mathbf{H}^H\mathbf{H}$, based on the delay-Doppler location of propagation paths, has either distinct or repetitive eigenvalues. When the number of distinct eigenvalues is less than equal two, we derive an exact closed form expression for the probability distribution function (pdf) of the ZF receiver SINR by assuming perfect receive CSI. We achieve this objective by i) exploiting structure of the OTFS channel matrix $\mathbf{H}$; and ii) using intricate mathematical results from probability theory. We subsequently derive closed form BER expressions by averaging the conditional BER expression over the SINR pdf. 2) When $\mathbf{H}^H\mathbf{H}$ has n distinct eigenvalues, we derive the SINR pdf by using numerical integration. We then show that the SINR pdf can be tightly approximated by Gamma pdf, which is then used to derive the tractable BER expression by averaging the conditional BER. 3) We extend the above derivations for the SINR pdf and BER for the imperfect receive CSI scenario also. We show that the BER calculated using these theoretical expressions perfectly match the one computed numerically for both perfect and imperfect receive CSI, and that too for dynamic high Doppler environment. These BER expressions which, unlike [20], do not require any averaging, and can be used by a system designer to benchmark the OTFS BER without performing time-consuming numerical simulations.

Notations: Lower and upper case boldface letters $\mathbf{a}$ and $\mathbf{A}$ denote vectors and matrices, respectively. The superscript $(\cdot)^H$ and $(\cdot)^T$ denote Hermitian and transpose operators respectively, and $\mathbf{A} \otimes \mathbf{B}$ denotes the Kronecker product of two matrices $\mathbf{A}$ and $\mathbf{B}$. The operator $\mathbb{E}[\cdot]$ represents the expectation of a random variable. The operation $[\mathbf{A}]_{(p,q)}$ extracts the (p,q)th element of the matrix $\mathbf{A}$, and $[\mathbf{D}]_{p,q}$ extracts the (p,q)th block of the matrix $\mathbf{D}$. The notations $\text{diag}[a_1, a_2, \ldots, a_N]$ and $\text{blkdiag}[\mathbf{A}_1, \mathbf{A}_2, \ldots, \mathbf{A}_N]$ denote a diagonal matrix and a block diagonal matrix, respectively.

The notations $\mathbf{I}_N$, $\mathbf{0}_{M\times N}$ and $[m-n]_M$ denote an $N\times N$ identity matrix, $M\times N$ zero matrix and modulo-M operation, respectively.

II. System Model

1) OTFS Transmitter: We consider an OTFS frame with MN delay-Doppler symbols, where M and N denote the number of delay and Doppler bins, respectively [14]. Let $x[k,l]$, for $0\le k\le N-1$ and $0\le l\le M-1$, be the QAM symbol on the kth Doppler and the lth delay bin in the OTFS delay-Doppler grid. The OTFS transmitter converts these delay-Doppler domain symbols into time-frequency domain by using the inverse symplectic finite Fourier transform (ISFFT) [14]. The symbol at the time index n and the frequency index m, which is denoted as $x_{\text{TF}}[n,m]$, is consequently given as [14]:

$$x_{\text{TF}}[n,m]=\frac{1}{MN}\sum_{k=0}^{N-1}\sum_{l=0}^{M-1}x[k,l]\exp\left\{j2\pi\Big(\frac{nk}{N}-\frac{ml}{M}\Big)\right\}.$$

Here $0\le n\le N-1$ and $0\le m\le M-1$. With a subcarrier spacing of $\Delta f=1/T$, the time-frequency domain OTFS frame has a duration NT with a bandwidth $M\Delta f$ [14]. The time-frequency domain symbols $x_{\text{TF}}[n,m]$ at the transmitter are then shaped using the pulse $g_{\text{tx}}(t)$, followed by the Heisenberg transform [14].

2) OTFS Receiver: The receiver performs Wigner transform on the noisy received signal by using a pulse $g_{\text{rx}}(t)$ that is matched to the transmit pulse $g_{\text{tx}}(t)$ [13]. The output of the Wigner transform is sampled at $t=nT$ and $f=m\Delta f$ which yields the following time-frequency domain signal [13]:

$$y_{\text{TF}}[n,m]=H[n,m]x_{\text{TF}}[n,m]+V[n,m]. \tag{1}$$

Here $V[n,m]$ denotes the additive white Gaussian noise at the output of Wigner transform, and

$$H[n,m]=\int_\nu\int_\tau h(\tau,\nu)\,e^{j2\pi\nu nT}e^{-j2\pi(\nu+m\Delta f)\tau}d\tau d\nu. \tag{2}$$

3) OTFS Channel: The two-dimensional parameter $h(\tau,\nu)$ in (2) denotes the delay-Doppler domain wireless channel with delay parameter τ and Doppler parameter ν. It is given as [14]

$$h(\tau,\nu)=\sum_{i=1}^{L_h}h_i\delta(\tau-\tau_i)\,\delta(\nu-\nu_i). \tag{3}$$

The scalar h_i is the complex channel gain with pdf $\mathcal{CN}(0,\sigma^2_{L_{h_i}})$ [13]. The term L_h gives the number of channel paths corresponding to the L_h clusters of reflectors in the wireless medium. The ith cluster introduces Doppler shift of ν_i and a delay of τ_i such that

$$\tau_i=\frac{l_i}{M\Delta f}\text{ and }\nu_i=\frac{k_i}{NT}, \tag{4}$$

where l_i and k_i respectively denote integer indices for the delay τ_i and Doppler ν_i [14].[1]

[1]Both delay and Doppler values need not be integer multiple of taps l_i and k_i [13]; their discretization, however, allows us to model the channel with fewer delay and Doppler taps [27].

The time-frequency domain signal $y_{\text{TF}}[n,m]$ undergoes the SFFT operation to yield the delay-Doppler domain signal using received signal as [14]:

$$y[k,l]=\sum_{n=0}^{N-1}\sum_{m=0}^{M-1}y_{\text{TF}}[n,m]\exp\left\{-j2\pi\Big(\frac{nk}{N}-\frac{ml}{M}\Big)\right\}.$$

By substituting $y_{\text{TF}}[n,m]$ and $x_{\text{TF}}[n,m]$, the delay-Doppler signal $y[k,l]$ can be expressed as [13]

$$y[k,l]=\sum_{i=1}^{L_h}h_i'x[(k-k_i)_N,(l-l_i)_M]+v[k,l]. \tag{5}$$

Here $h_i'=h_i\exp(-j2\pi\nu_i\tau_i)$ and $v[k,l]$ is the circularly symmetric zero mean complex Gaussian noise with variance σ_v^2. Note that since $h_i\sim\mathcal{CN}(0,\sigma^2_{h_i})$, so is h_i'. The SISO-OTFS receive signal in (5), for mathematical brevity, is expressed in the vector form as follows [11], [28]:

$$\mathbf{y}=\mathbf{H}\mathbf{x}+\mathbf{v}. \tag{6}$$

The $(k+Nl)$th element of $\mathbf{x}\in\mathbb{C}^{MN\times1}$, for $0\le k\le N-1$ and $0\le l\le M-1$, satisfies the condition $x_{k+Nl}=x[k,l]$. The noise vector $\mathbf{v}\in\mathbb{C}^{MN\times1}$ and the received vector $\mathbf{y}\in\mathbb{C}^{MN\times1}$ also have the same structure. The elements of $\mathbf{v}$ are independent and identically distributed (i.i.d.) with pdf $\mathcal{CN}(0,\sigma_v^2)$. The elements of $\mathbf{x}$ are also i.i.d with zero mean and variance P_x [1]. The OTFS channel $\mathbf{H}\in\mathbb{C}^{MN\times MN}$ is a doubly-block circulant matrix – a block circulant matrix with M circulant blocks, wherein each block of size $N\times N$ is a circulant matrix [28]. We next state a lemma, which is proved in Appendix A.

Lemma 1: Let $\mathcal{C}_{M,N}$ be a set of circulant matrices with M circulant blocks with each block of size $N\times N$ being a circulant matrix. This implies that if a matrix $\mathbf{H}\in\mathcal{C}_{M,N}$, it can be written as $\mathbf{H}=\texttt{CIRC}(\mathbf{A}_0,\mathbf{A}_1,\ldots,\mathbf{A}_{M-1})$, where $\texttt{CIRC}(\cdot)$ denotes the circulant operation and $\mathbf{A}_i\in\mathbb{C}^{N\times N}$ gives the ith circulant block. If a matrix $\mathbf{H}\in\mathcal{C}_{M,N}$, it can be diagonalized as

$$\mathbf{H}=(\mathbf{F}_M\otimes\mathbf{F}_N)^H\mathbf{D}(\mathbf{F}_M\otimes\mathbf{F}_N), \tag{7}$$

where $\mathbf{F}_M\in\mathbb{C}^{M\times M}$ and $\mathbf{F}_N\in\mathbb{C}^{N\times N}$ are the normalized DFT matrices, and the diagonal matrix $\mathbf{D}\in\mathbb{C}^{MN\times MN}$ comprises of eigenvalues $\lambda_1,\lambda_2,\ldots,\lambda_{MN}$ of the matrix $\mathbf{H}$. It can be expressed by defining $W_M=e^{j2\pi/M}$ as

$$\mathbf{D}=\text{blkdiag}\left[\sum_{i=0}^{M-1}\mathbf{D}_i,\sum_{i=0}^{M-1}W_M^i\mathbf{D}_i,\ldots,\sum_{i=0}^{M-1}W_M^{i(M-1)}\mathbf{D}_i\right]. \tag{8}$$

The diagonal matrix $\mathbf{D}_i\in\mathbb{C}^{N\times N}$ contains eigenvalues of the ith circulant block $\mathbf{A}_i$.

The OTFS channel matrix in (6) can now be decomposed using *Lemma* 1 as follows

$$\mathbf{H}=\mathbf{\Psi}^H\mathbf{D}\mathbf{\Psi}. \tag{9}$$

Here $\mathbf{\Psi}=\mathbf{F}_M\otimes\mathbf{F}_N\in\mathbb{C}^{MN\times MN}$. It is easy to see that $\mathbf{\Psi}\mathbf{\Psi}^H=\mathbf{\Psi}^H\mathbf{\Psi}=\mathbf{I}_{MN}$. The bi-orthogonal pulse shaping, irrespective of the Doppler value of each path, makes the OTFS channel $\mathbf{H}$ a doubly-block circulant matrix – a

block circulant matrix with M circulant blocks, each of size $N \times N$ [11], [13], [28]. The OTFS channel matrix $\mathbf{H}$, as shown above, can be diagonalized using FFT matrices [11].

Remark 1: We consider, as commonly assumed in the literature [10], [11], [13], [19], the transmit and receiver pulses which satisfy bi-orthogonality and robustness conditions [10]. We note that the current work is the first one to analytically derive the BER of OTFS ZF receivers. One may be interested in evaluating the performance of OTFS ZF receiver designed with practical pulse. The proposed analysis will lower bound the performance of such designs. Analysis for BER of OTFS ZF receiver design with practical pulse is beyond the scope of this paper, but eventually this needs to be considered as future work.

Remark 2: For a static multipath channel, as explained in [29], OTFS and asymmetric-OFDM (A-OFDM) share a common transceiver structure. The system model for A-OFDM system is given as $\mathbf{y} = \mathbf{H}_{\text{eff}}\mathbf{x} + \mathbf{w}$ [29], where the time domain channel matrix $\mathbf{H}_{\text{eff}}$ has a block-diagonal structure as $\mathbf{H}_{\text{eff}} = \text{blkdiag}\big[\mathbf{H}_0, \mathbf{H}_1, \ldots, \mathbf{H}_{N-1}\big]$. Here each block is a circulant matrix of sized $M \times M$, which can be diagonalised using DFT matrices [29]. Since the entries of $\mathbf{H}_i$ in a row/column are zero mean i.i.d. complex Gaussian. The ZF receiver SINR, therefore, has Chi-square distribution. The theoretical BER expression for A-OFDM system can be easily derived by using the methods used for deriving the BER of the OFDM ZF receiver whose SINR is also Chi-square distributed [30], [31]. However, the current work focuses on rapidly time varying channel that supports a vehicular speed of the order of 500 kmph. The current work detects data in the delay-Doppler domain, wherein the channel matrix $\mathbf{H}$, unlike that of $\mathbf{H}_{\text{eff}}$ in an A-OFDM system, has a doubly block circulant structure. Consequently ZF SINR herein, as also shown in the sequel, does not follow the Chi-square pdf, except for the simple case of only one delay-Doppler propagation path between the OTFS transmitter and receiver.

III. Derivation of Closed Form BER Expression for ZF OTFS Receivers

The ZF receiver is commonly used in OFDM systems in the frequency domain for low-to-moderate time varying channel. Its effectiveness therein, however, reduces for highly time-varying channels [9], [11]. This happens due to the large number of rapidly time-varying dominant paths in the time-frequency domain [32, Fig. 1], which causes large inter-carrier-interference in an OFDM system. A ZF receiver is a reasonable choice for OTFS systems with delay-Doppler domain receive processing, wherein the number of dominant channel paths is significantly lower than the time-frequency domain [32, Fig. 1]. The delay-Doppler domain channel appears time invariant for a longer duration than its time-frequency domain counterpart [32]. A ZF receiver for OTFS systems, due to these reasons has a reasonable performance, and has therefore been investigated by many recent works [11], [20]–[22]. We next derive the BER expression for the ZF receiver by first calculating the SINR, and then its pdf. We derive the SINR by assuming perfect receive CSI, and later derive SINR for the imperfect CSI case also.

A. SINR and BER Calculation With Perfect Receive CSI

The ZF receiver for the system model in (6) can be expressed as follows [33]: $\mathbf{G}_{\text{A}} = \mathbf{H}\big(\mathbf{H}^H\mathbf{H}\big)^{-1}$. The estimate of $\mathbf{x}$ is consequently $\hat{\mathbf{x}} = \mathbf{G}_{\text{A}}^H\mathbf{y} = \mathbf{x} + \mathbf{w}$. Here $\mathbf{w} = \big(\mathbf{H}^H\mathbf{H}\big)^{-1}\mathbf{H}^H\mathbf{v}$ is the equivalent noise with covariance matrix $\mathbf{C}_{\mathbf{w}} = \mathbb{E}[\mathbf{w}\mathbf{w}^H] = \sigma_v^2\big(\mathbf{H}^H\mathbf{H}\big)^{-1}$. The SINR of the kth symbol of the transmit vector $\mathbf{x}$ is therefore

$$\gamma_k = \frac{\mathbb{E}[|\mathbf{x}_{\text{k}}|^2]}{\sigma_v^2\big[\big(\mathbf{H}^H\mathbf{H}\big)^{-1}\big]_{k,k}} = \frac{\rho}{\big[\big(\mathbf{H}^H\mathbf{H}\big)^{-1}\big]_{k,k}}. \tag{10}$$

The scalar $\rho = P_x/\sigma_v^2$ denotes the SNR. We next calculate the pdf of γ_k, which is subsequently used to derive a closed form BER expression. Before doing that a remark is in order.

Remark 3: The received symbol vector for a conventional MIMO/MIMO-OFDM system is $\mathbf{y}_{\text{mimo}} = \mathbf{H}_{\text{mimo}}\mathbf{x}_{\text{mimo}} + \mathbf{v}_{\text{mimo}}$ [30]. This system will also have the same SINR expression for the kth symbol of the ZF receiver as in (10). It is, therefore, important to differentiate the present work from its counterpart in the MIMO-OFDM literature [30], [31], [34], [35]. The entries of MIMO OFDM channel matrix $\mathbf{H}_{\text{mimo}} \in \mathbb{C}^{N_r \times N_t}$, while deriving the BER of ZF receivers, are commonly assumed to be spatially uncorrelated/correlated complex Gaussian random variables [30], [31], [34], [35]. For $\mathbf{H}_{\text{mimo}}$ with uncorrelated entries, the matrix product $\mathbf{H}_{\text{mimo}}^H\mathbf{H}_{\text{mimo}}$ follows the well-known Wishart distribution [30]. The random variable $1/\big[(\mathbf{H}_{\text{mimo}}^H\mathbf{H}_{\text{mimo}})^{-1}\big]_{k,k}$ in the SINR expression consequently has Chi-square pdf with $2(N_r - N_t + 1)$ degrees of freedom [30], [31]. For correlated $\mathbf{H}_{\text{mimo}}$, the term $1/\big[(\mathbf{H}_{\text{mimo}}^H\mathbf{H}_{\text{mimo}})^{-1}\big]_{k,k}$ has weighted Chi-square pdf [34], [35]. The Chi-square pdf in a MIMO-OFDM system leads to tractable BER expression [30], [31], [34], [35]. For OTFS systems, due to delay-Doppler signal processing, the channel matrix $\mathbf{H} \in \mathbb{C}^{MN \times MN}$ in (10) has sparse doubly-circulant structure with correlated entries [11]. The $1/\big[(\mathbf{H}^H\mathbf{H})^{-1}\big]_{k,k}$ in (10), as shown in the sequel, does not follow the Chi-square pdf, except for the case with only one delay-Doppler propagation path between the OTFS transmitter and receiver. The SINR pdf and corresponding BER derivations in the present work are, therefore, completely different than MIMO-OFDM systems in [30], [31], [34], [35].

The SINR expression in (10) can be expressed using the decomposition in (9) as follows:

$$\gamma_k = \frac{\rho}{\big[\mathbf{\Psi}^H(\mathbf{D}^H\mathbf{D})^{-1}\mathbf{\Psi}\big]_{k,k}}. \tag{11}$$

With $\mathbf{H} = \mathbf{\Psi}^H\mathbf{D}\mathbf{\Psi}$ from (9), $\mathbf{H}^H\mathbf{H} = \mathbf{\Psi}^H\mathbf{D}^H\mathbf{D}\mathbf{\Psi}$. Since $\mathbf{D}$ contains eigenvalues of $\mathbf{H}$, the matrix product $\mathbf{D}^H\mathbf{D}$ consists of eigenvalues of the matrix $\mathbf{H}^H\mathbf{H}$. By exploiting the fact that $\mathbf{\Psi}$ is a unitary matrix, and that $\mathbf{D} = \text{diag}[\lambda_1, \lambda_2, \ldots, \lambda_{MN}]$, the expression of γ_k for $1 \leq k \leq MN$ can be simplified as follows

$$\gamma = \frac{\rho}{\frac{1}{MN}\left(\frac{1}{|\lambda_1|^2} + \frac{1}{|\lambda_2|^2} + \ldots + \frac{1}{|\lambda_{MN}|^2}\right)} = \rho MN\phi. \tag{12}$$

The subscript k is dropped in (12) as the statistical characteristics of SINR γ_k, as shown in the sequel, are identical for

all k symbols. In the above expression, the random variable

$$\phi = \left(\sum_{i=1}^{MN} \frac{1}{|\lambda_i|^2} \right)^{-1}. \tag{13}$$

Reference [36] derived the BER expression for an AWGN channel. References [30, Eq. (18)], [37, Eq. (62)], by using the AWGN BER, derived the instantaneous BER expression for $\mathcal{M}$-QAM for fading channel as in (14), as shown at the bottom of the page, where the constant $C_{\mathcal{M}} = \frac{2}{\sqrt{\mathcal{M}} \log_2 \sqrt{\mathcal{M}}}$ and the variable $\psi(i,k)$ is expressed as

$$\psi(i,k) = (-1)^{\left\lfloor \frac{i.2^{k-1}}{\sqrt{\mathcal{M}}} \right\rfloor} \left(2^{k-1} - \left\lfloor \frac{i.2^{k-1}}{\sqrt{\mathcal{M}}} - \frac{1}{2} \right\rfloor \right). \tag{15}$$

The average BER of the ZF OTFS receiver is next calculated by averaging the expression in (14) over the random variable γ as follows

$$P_{\text{ZF}} = \int_0^\infty P_b f_\gamma(\gamma)\, d\gamma. \tag{16}$$

Here $f_\gamma(\gamma)$ is the pdf of the SINR γ. For 4-QAM, the BER expression can be simplified as follows: $P_{\text{ZF}} = \int_0^\infty Q\left(\sqrt{\gamma}\right) f_\gamma(\gamma)\, d\gamma$ [1]. We see from (16) that to calculate the BER, we need to derive the SINR pdf $f_\gamma(\gamma)$, which is a challenging task. For example, the authors in [20] derived semi-theoretical BER for MIMO-OTFS systems and avoided SINR pdf derivation by averaging conditional BER over multiple channel realization. This makes their BER expression computationally-inefficient as the SINR needs to be calculated for each channel realization.

We next derive the pdf $f_\gamma(\gamma)$. The SINR γ, as observed from (12), is a function of random variable ϕ with pdf $f_\phi(\phi)$, which in turn is a function of the eigenvalues λ_i of the OTFS channel matrix $\mathbf{H}$. We now state the following lemma, whose proof is relegated to Appendix B.

Lemma 2: Each element of the diagonal matrix $\mathbf{D}$ is identically distributed as $\mathcal{CN}(0, \sigma^2)$, where $\sigma^2 = (1/L_h) \sum_{i=1}^{M} L_h^i$ with L_h^i being the number of non-zero entries in a column or row of the ith circulant block of $\mathbf{H}$.

It follows from *Lemma* 2 that $|\lambda_i|^2$ has exponential pdf with a rate parameter $1/\sigma^2$. Consequently, $|\lambda_i|^{-2}$ has inverse Gamma pdf with unity shape parameter and the scale parameter σ^2 [38]. *The random variable ϕ is thus the inverse of sum of MN inverse Gamma random variables.*

As shown in Appendix B, the diagonal matrix $\mathbf{D}_i$ in (8) is calculated as $\mathbf{D}_i = \text{diag}[\bar{\mathbf{F}}_N \mathbf{H}_i(:,1)]$, where $\bar{\mathbf{F}}_N \in \mathbb{C}^{N \times N}$ is the DFT matrix, and $\mathbf{H}_i(:,1) \in \mathbb{C}^{N \times 1}$ is the first column of the ith circulant block of $\mathbf{H}$. The entries λ_l^i of $\mathbf{D}_i$, as explained below, can be distinct or repetitive. This depends on the number of non-zero values in $\mathbf{H}_i(:,1)$ which, as shown in (5), depends on the delay-Doppler locations of propagation paths. For example, all entries of $\mathbf{D}_i$ are identical, if $\mathbf{H}_i(:,1)$ has only one non-zero entry, which is at the first location. The elements of $\mathbf{D}$ in (8), which consists of the eigenvalues $\lambda_i, \lambda_2, \ldots, \lambda_{MN}$ of $\mathbf{H}$, can thus be repetitive or distinct, or a combination of both. Also, if λ_i values differ only by a phase factor, entries of $\mathbf{D}^H\mathbf{D}$ i.e., $|\lambda_1|^2, |\lambda_2|^2, \ldots, |\lambda_{MN}|^2$ will be same. Consequently, the inverse Gamma random variables $1/|\lambda_i|^2$ in (13) can be distinct or repetitive or combination of both. Depending upon the nature of eigenvalues of $\mathbf{H}^H\mathbf{H}$, we divide our BER analysis into the following three parts.

1) All Eigenvalues of $\mathbf{H}^H\mathbf{H}$ Are Identical: This implies that $\mathbf{D}^H\mathbf{D}$ has identical entries. It can be readily verified using (8) and the relation $\mathbf{D}_i = \text{diag}[\bar{\mathbf{F}}_N \mathbf{H}_i(:,1)]$ that this condition arises when the number of channel paths $L_h = 1$. This happens irrespective of the delay-Doppler locations, and the values of delay bins M and Doppler bins N. For example, with $L_h = 1$, $N = 2$, $M = 2$, and $l_i = 0$, $k_i = 1$, the OTFS channel matrix $\mathbf{H}$ for one realization is given in (17), as shown at the bottom of the page. With $M = N = 2$, the matrix $\mathbf{H}$ has two circulant blocks $\mathbf{A}_0$ and $\mathbf{A}_1$. They can be readily identified from (17) as in (18), as shown at the bottom of the page. We see that both $\mathbf{A}_0$ and $\mathbf{A}_1$ are circulant matrices, which also circulate in $\mathbf{H}$. Using the property that eigenvalues of a circulant matrix are the DFT of its first column [51], the eigenvalues of $\mathbf{A}_0$ and $\mathbf{A}_1$ are calculated as $\mathbf{D}_0 = \text{diag}[\mathbf{F}_2 \mathbf{A}_0(:,1)] = \text{diag}[0.2174 + 0.5814i, -0.2174 - 0.5814i]$ and $\mathbf{D}_1 = \text{diag}[\mathbf{F}_2 \mathbf{A}_1(:,1)] = \text{diag}[0,0]$, respectively. By substituting $\mathbf{D}_0$ and $\mathbf{D}_1$ in (8), the eigenvalue matrix of $\mathbf{H}$ can be computed $\mathbf{D} = \text{blkdiag}[\mathbf{D}_0, W_2^0\ \mathbf{D}_0]$. Thus, we have

$$\mathbf{D}^H\mathbf{D} = \begin{bmatrix} 0.3853 & 0.0000 & 0.0000 & 0.0000 \\ 0.0000 & 0.3853 & 0.0000 & 0.0000 \\ 0.0000 & 0.0000 & 0.3853 & 0.0000 \\ 0.0000 & 0.0000 & 0.0000 & 0.3853 \end{bmatrix}.$$

$$P_b = C_{\mathcal{M}} \sum_{k=1}^{\log_2 \sqrt{\mathcal{M}}} \sum_{i=0}^{(1-2^{-k})\sqrt{\mathcal{M}}-1} \psi(i,k) Q\left((2i+1) \sqrt{\frac{3\gamma}{\mathcal{M}-1}} \right). \tag{14}$$

$$\mathbf{H} = \begin{bmatrix} 0.0000 + 0.0000i & 0.2174 + 0.5814i & 0.0000 + 0.0000i & 0.0000 + 0.0000i \\ 0.2174 + 0.5814i & 0.0000 + 0.0000i & 0.0000 + 0.0000i & 0.0000 + 0.0000i \\ 0.0000 + 0.0000i & 0.0000 + 0.0000i & 0.0000 + 0.0000i & 0.2174 + 0.5814i \\ 0.0000 + 0.0000i & 0.0000 + 0.0000i & 0.2174 + 0.5814i & 0.0000 + 0.0000i \end{bmatrix} \tag{17}$$

$$\mathbf{A}_0 = \begin{bmatrix} 0.0000 + 0.0000i & 0.2174 + 0.5814i \\ 0.2174 + 0.5814i & 0.0000 + 0.0000i \end{bmatrix}, \quad \mathbf{A}_1 = \begin{bmatrix} 0.0000 + 0.0000i & 0.0000 + 0.0000i \\ 0.0000 + 0.0000i & 0.0000 + 0.0000i \end{bmatrix} \tag{18}$$

We see that $|\lambda_1|^2 = |\lambda_2|^2 = \ldots = |\lambda_{MN}|^2 = |\lambda|^2 = 0.3853$. The SINR γ in (12) is therefore

$$\gamma = \frac{\rho MN}{MN/|\lambda|^2} = \rho|\lambda|^2. \tag{19}$$

We accordingly have $\phi = |\lambda|^2$, which has an exponential pdf $f_\phi(\phi) = \frac{1}{\sigma^2}\exp(-\phi/\sigma^2)$. The SINR γ, consequently, has exponential pdf with the rate parameter $1/\rho\sigma^2$, i.e., $f_\gamma(\gamma) = \frac{1}{\rho\sigma^2}\exp(-\gamma/\rho\sigma^2)$. To compute the BER for this case, we state the next Lemma, which is proved in Appendix C.

Lemma 3: When eigenvalues of $\mathbf{H}^H\mathbf{H}$ are identical, the BER of ZF OTFS receiver is

$$P_{\text{ZF}} = C_{\mathcal{M}} \sum_{k=1}^{\log_2\sqrt{\mathcal{M}}} \sum_{i=0}^{(1-2^{-k})\sqrt{\mathcal{M}}-1} \frac{\Psi(i,k)}{2} \times \left[1 - \sqrt{\frac{(2i+1)^2 3\rho\sigma^2}{2(\mathcal{M}-1) + (2i+1)^2 3\rho\sigma^2}}\right]. \tag{20}$$

For 4-QAM, the above BER expression, by using the expression in (15), simplifies as

$$P_{\text{ZF}_{\text{QPSK}}} = \frac{1}{2}\left[1 - \sqrt{\frac{\rho\sigma^2}{2+\rho\sigma^2}}\right]. \tag{21}$$

We next consider the case, wherein the matrix $\mathbf{H}^H\mathbf{H}$ has two distinct eigenvalues.

2) $\mathbf{H}^H\mathbf{H}$ Has Two Distinct Eigenvalues: The diagonal matrix $\mathbf{D}^H\mathbf{D}$ now has two distinct entries. Using (8) and the relation $\mathbf{D}_i = \text{diag}[\bar{\mathbf{F}}_N\mathbf{H}_i(:,1)]$, we see that this case arises when $L_h = N = 2$ and both the delay-Doppler propagation paths lie in a single circulant block of $\mathbf{H}$. For this case, we get, $|\lambda_1|^2 = |\lambda_3|^2 = \ldots = |\lambda_{MN-1}|^2 = |\lambda_1|^2$ and $|\lambda_2|^2 = |\lambda_4|^2 = \ldots = |\lambda_{MN}|^2 = |\lambda_2|^2$. For example, with $N = L_h = 2$, $M = 8$, $l_i = [0,0]$ and $k_i = [0,1]$, $\mathbf{H}^H\mathbf{H}$ for a particular realization has only two independent distinct eigenvalues: $|\lambda_1|^2 = 0.8774$ and $|\lambda_2|^2 = 0.4333$. We next derive a closed form BER expression for this case.

When $\mathbf{D}^H\mathbf{D}$ has only two distinct eigenvalues, the SINR γ from (12) simplifies as

$$\gamma = \frac{\rho MN}{\frac{MN}{2}\left(\frac{1}{|\lambda_1|^2} + \frac{1}{|\lambda_2|^2}\right)} = 2\rho\phi. \tag{22}$$

The random variable ϕ is now given as

$$\phi = \frac{|\lambda_1|^2|\lambda_2|^2}{|\lambda_1|^2 + |\lambda_2|^2} = Z|\lambda_2|^2. \tag{23}$$

The random variable $Z = \frac{|\lambda_1|^2}{|\lambda_1|^2+|\lambda_2|^2}$. Since $|\lambda_1|^2 \sim \text{Exp}(1/\sigma_1^2)$ and $|\lambda_2|^2 \sim \text{Exp}(1/\sigma_2^2)$ with $\sigma_1^2 = \sigma_2^2 = \sigma^2$, Z is uniformly distributed between 0 and 1 [39], which is equivalent to Beta distribution: $Z \sim \text{B}(1,1)$. The exponential pdf can be expressed as Gamma pdf: $|\lambda_2|^2 \sim \text{G}(1,\sigma^2)$. The random variable ϕ is, therefore, a product of Beta and Gamma random variables. Its pdf is therefore [40]:

$$f_\phi(\phi) = \frac{1}{\sigma^2}\exp\left(-\frac{\phi}{\sigma^2}\right)\boldsymbol{\psi}\left(1,1;\frac{\phi}{\sigma^2}\right). \tag{24}$$

Here $\psi(\cdot)$ is the Kummer function, which is defined as [40]

$$\boldsymbol{\psi}(a,b;x) = \frac{1}{\Gamma(a)}\int_0^\infty \exp(-xt)t^{a-1}(1+t)^{b-a-1}dt, \tag{25}$$

where $\Gamma(a)$ is the gamma function. Substituting $\boldsymbol{\psi}(a,b;x)$ with $a = b = 1$ and $x = \phi/\sigma^2$ in (24), pdf of ϕ is

$$f_\phi(\phi) = \frac{1}{\sigma^2}\exp\left(-\frac{\phi}{\sigma^2}\right)\int_0^\infty \frac{\exp\left(-\frac{\phi}{\sigma^2}t\right)}{(1+t)}dt = \frac{1}{\sigma^2}\text{E}_1\left(\frac{\phi}{\sigma^2}\right), \tag{26}$$

where $\text{E}_1\left(\phi/\sigma^2\right)$ denotes the exponential integral function [41, pp. 6]. Since $\gamma = 2\rho\phi$, the pdf of SINR γ can be obtained as

$$f_\gamma(\gamma) = \frac{1}{2\rho\sigma^2}\text{E}_1\left(\frac{\gamma}{2\rho\sigma^2}\right). \tag{27}$$

For the BER expression, we provide the following lemma, whose proof is given in Appendix D

Lemma 4: When $\mathbf{H}^H\mathbf{H}$ has only two distinct eigenvalues, the BER of ZF OTFS receiver is

$$P_{\text{ZF}} = C_{\mathcal{M}} \sum_{k=1}^{\log_2\sqrt{\mathcal{M}}(1-2^{-k})\sqrt{\mathcal{M}}-1} \sum_{i=0} \Psi(i,k) \times \left[\frac{1}{2} - \frac{1}{4\rho\sigma^2}\left\{\frac{1}{a}\left(1+\frac{a}{b}\right)^{\frac{1}{2}} + \frac{1}{2b}\ln\left(\frac{\sqrt{a+b}-\sqrt{b}}{\sqrt{a+b}+\sqrt{b}}\right)\right\}\right],$$

where the parameters $a = \frac{1}{2\rho\sigma^2}$ and $b = \frac{(2i+1)^2 3}{2(\mathcal{M}-1)}$.
For 4-QAM symbols ($\mathcal{M} = 4$), the above BER expression is simplified as in (28), as shown at the bottom of the page.

3) $\mathbf{H}^H\mathbf{H}$ Has n Distinct Eigenvalues: We now consider the case when $\mathbf{H}^H\mathbf{H}$ has n distinct eigenvalues. The diagonal $\mathbf{D}^H\mathbf{D}$ matrix, therefore, has n distinct entries. We show that ϕ in (13), and hence the SINR $\gamma = \rho MN\phi$, is a function of inverse of the weighted sum of inverted Gamma random variables, whose pdf is not straightforward to derive [42]. We use numerical integration to derive pdf of the SINR γ.

Let the n distinct entries of $\mathbf{D}^H\mathbf{D}$ be $|\lambda_1|^2, |\lambda_2|^2, \ldots, |\lambda_n|^2$. The ith distinct entry repeats C_i times such that $C_1 + C_2 + \cdots C_n = MN$. The random variable ϕ in (13) can be written as

$$\phi = \left(\sum_{i=1}^n \frac{C_i}{|\lambda_i|^2}\right)^{-1} = (X)^{-1}.$$

$$P_{\text{ZF}_{\text{QPSK}}} = \frac{1}{2}\left[1 - \left\{\left(1+\frac{1}{\rho\sigma^2}\right)^{\frac{1}{2}} + \frac{1}{2\rho\sigma_2^2}\ln\left(\frac{\sqrt{1+\rho\sigma_2^2}-\sqrt{\rho\sigma_2^2}}{\sqrt{1+\rho\sigma_2^2}+\sqrt{\rho\sigma_2^2}}\right)\right\}\right]. \tag{28}$$

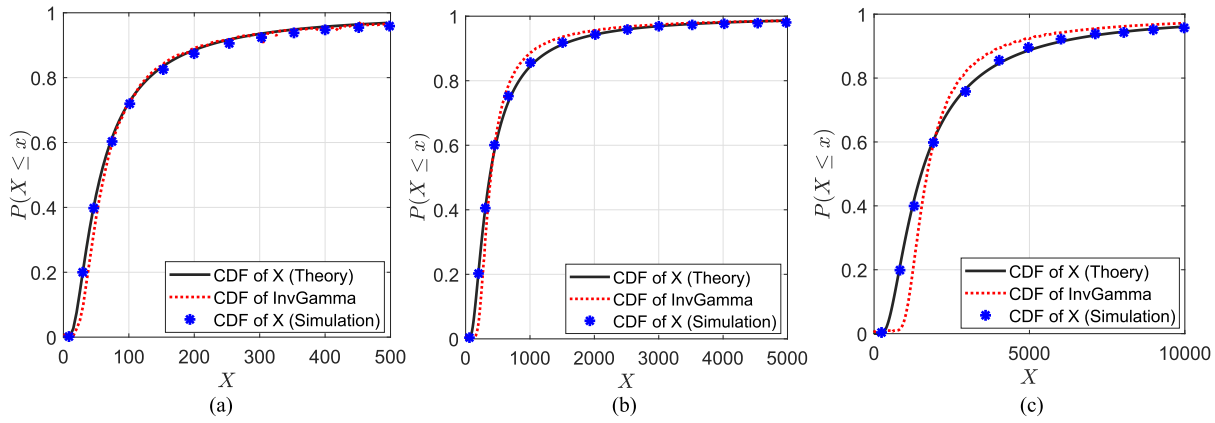

Fig. 1. Comparison of theoretical CDF of X in (31) with that of its simulated counterpart with (a) 16 distinct λ_is with $M = N = 8$ and $L_h = 3$; (b) 72 distinct λ_is with $M = N = 12$ and $L_h = 4$; and (c) 256 distinct λ_i with $M = N = 16$ and $L_h = 5$. The above plots also compare the two CDFs with that of an inverted Gamma random variable for a study in the sequel.

The eigenvalue λ_i, as shown in Appendix B, has pdf $\mathcal{CN}(0, \sigma_i^2)$. The random variable $X = \sum_{i=1}^{n} X_i = \sum_{i=1}^{n} C_i |\lambda_i|^{-2}$ is therefore the weighted sum of inverted Gamma random variables. It follows from [43] that the CDF of linear combination of inverted Gamma random variables can be computed as

$$F_X(x) = P(X \leq x) = \frac{1}{2} - \frac{1}{\pi} \int_0^{\infty} \Im \left(\frac{e^{-iux} \phi_X(u)}{u} \right) du. \tag{29}$$

The characteristics function $\phi_X(u)$ of X is derived in Appendix E. It is shown in [43] that the integrand

$$\lim_{u \to 0} \Im \left(\frac{e^{-iux} \phi_x(u)}{u} \right) = \sum_{i=1}^{n} \frac{C_i}{(\alpha_i - 1)\beta_i} - x. \tag{30}$$

Here α_i and β_i denote the shape and scale parameters of the random variable $|\lambda_i|^{-2}$. As shown in Appendix E, $|\lambda_i|^{-2} \sim \text{InvGamma}\left(1, 1/\sigma_i^2\right)$, which implies that $\alpha_i = 1$ and $\beta_i = 1/\sigma_i^2$. We see from (30) that the limit does not exist and the result of the integral in (29) becomes extremely complicated [43]. Consequently, when $n > 2$, it is analytically challenging to derive the exact pdf of X and ϕ [42]. We next use numerical integration method to evaluate the integral in (29) for deriving the pdf of X. As shown in Appendix E, by using the trapezoidal rule of numerical integration with maximum allowable error ε [43], an approximate expression for the CDF of X with characteristics function $\Phi_X(\cdot)$ is given as in (31), as shown at the bottom of the page. The parameter $\Delta > 0$ in (31) is chosen such that

$$\max \left[\Pr\left(X \leq x - \frac{2\pi}{\Delta} \right), \Pr\left(X \leq x + \frac{2\pi}{\Delta} \right) \right] < \frac{\varepsilon}{2}. \tag{32}$$

The parameter K in (31) is computed such that

$$\frac{1}{\pi} \sum_{k=K+1}^{\infty} \Im \left[\frac{\exp\left\{-i(k+\frac{1}{2})\Delta x\right\} \Phi_X\left\{(k+\frac{1}{2})\Delta\right\}}{(k+\frac{1}{2})} \right] < \frac{\varepsilon}{2}. \tag{33}$$

We see that the parameter K truncates the summation in (31) such that the truncation error is less then $\frac{\varepsilon}{2}$. Figure 1 compares the theoretical CDF of X in (31) with its simulated counterpart, which matches for different number of distinct eigenvalues λ_i. This shows the accuracy of the CDF expression in (31).

The pdf of X is derived by differentiating (31) w.r.t x as

$$f_X(x) = \frac{1}{\pi} \sum_{k=0}^{K} \Re \left[\Delta \exp\left\{ -i \left(k + \frac{1}{2} \right) \Delta x \right\} \Phi_X\left\{ \left(k + \frac{1}{2} \right) \Delta \right\} \right]. \tag{34}$$

We next derive the BER using the above pdf and simplified the BER derivation to a point where it requires solution of the integral $\int_0^{\infty} \cos(uy) dy$. Since this integral does not converge [43], it is difficult to further simplify the BER expression using the pdf in (34). We handle this problem by approximating the above pdf as inverted Gamma pdf, which yields a tractable closed form BER expression. Before performing this study, we observe from Fig. 1 that the CDF of inverted Gamma random variable in fact matches well with that of X.

a) BER derivation with pdf in (34)*:* To begin with, the SINR expression in (12) is re-written using the relation $\phi = 1/X$ as

$$\gamma = \frac{\rho MN}{X}. \tag{35}$$

$$\Pr(X \leq x) \approx \frac{1}{2} - \frac{1}{\pi} \sum_{k=0}^{K} \Im \left[\frac{\exp\left\{-i\left(k+\frac{1}{2}\right)\Delta x\right\} \Phi_X\left\{\left(k+\frac{1}{2}\right)\Delta\right\}}{\left(k+\frac{1}{2}\right)} \right]. \tag{31}$$

The BER, as shown in [42, Eq. (4)], can be derived by solving the integral

$$P_{\text{ZF}} = \int_0^\infty Q\left(\frac{1}{\sqrt{y}}\right) f_{1/\gamma}(y)dy, \tag{36}$$

where $f_{1/\gamma}(y)$ denotes pdf of the inverse SINR $1/\gamma$. We see from (35) that the inverse SINR $\frac{1}{\gamma} = qX$, where $q = \frac{1}{\rho MN}$. The pdf $f_{1/\gamma}(y) = \frac{1}{q} f_X\left(\frac{y}{q}\right)$. BY substituting $f_{1/\gamma}(y)$ in (36), the BER can be expressed as $P_{\text{ZF}} = \int_0^\infty Q\left(\frac{1}{\sqrt{qx}}\right) f_X(x)dx$. Substituting $f_X(x)$ from (34), we get

$$P_{\text{ZF}} = \int_0^\infty Q\left(\frac{1}{\sqrt{qx}}\right) \frac{1}{\pi} \sum_{k=0}^{K} \text{Re}\Bigg[\Delta \exp\left\{-i\left(k+\frac{1}{2}\right)\Delta x\right\} \Phi_X\left\{\left(k+\frac{1}{2}\right)\Delta\right\}\Bigg] dx. \tag{37}$$

By replacing $\left(k+\frac{1}{2}\right)\Delta = u_k$ and $Q(x) = \frac{1}{2}\text{erfc}(\frac{1}{\sqrt{2x}})$ and by rewriting the characteristic function as $\Phi_X(\cdot) = \Phi_{\text{R}}(\cdot) + i\Phi_{\text{I}}(\cdot)$ with $\Phi_{\text{R}}(\cdot)$ and $\phi_{\text{I}}(\cdot)$ being the real and imaginary parts of $\Phi_X(\cdot)$ respectively, the expression in (37) can be re-expressed as in (38), as shown at the bottom of the page, where the term $\text{I}_1 = \int_0^\infty \text{erfc}\left(\frac{1}{\sqrt{2qx}}\right)\cos(u_k x)dx$ and $\text{I}_2 = \int_0^\infty \text{erfc}\left(\frac{1}{\sqrt{2qx}}\right)\sin(u_k x)dx$. It follows from [44, page 12] that

$$\text{I}_2 = -\frac{1}{u_k} e^{-\left(\frac{u_k}{q}\right)^{1/2}} \sin\left[\left(\frac{u_k}{q}\right)^{1/2}\right], \quad \text{and}$$

$$\text{I}_1 = \int_0^\infty \left\{1 - \text{erf}\left(\frac{1}{\sqrt{2qx}}\right)\right\}\cos(u_k x)dx = \int_0^\infty \cos(u_k x)dx - \frac{1}{u_k} e^{-\left(\frac{u_k}{q}\right)^{1/2}} \cos\left[\left(\frac{u_k}{q}\right)^{1/2}\right].$$

We see that the term I_1 above does not have a closed form solution as the integral $\int_0^\infty \cos(ux)dx$ does not converge [43]. A closed form BER expression is difficult to derive using the pdf in (34). We overcome this challenge by approximating the pdf as discussed next.

b) BER derivation with approximated pdf: We observe from Fig. 1, where we have plotted the CDF of X, that for different numbers of distinct eigenvalues of $\mathbf{H}$, the CDF of X closely follows the CDF of an inverted Gamma random variable. The pdf $f_X(x)$ in (34) can therefore approximated as the inverted Gamma pdf. Consequently, the pdf of SINR $\gamma = \frac{\rho MN}{X}$ in (35) can be approximated as Gamma pdf. We will later show that this approximation leads to a tractable BER expression, which closely follows its numerical counterpart.

Let the CDF of X be approximated by that of inverse Gamma random variable with shape parameter a and scale parameter b^{-1}. We, therefore, have [38]:

$$F_X(x; a, b^{-1}) \approx \frac{\Gamma\left(a, \frac{b^{-1}}{x}\right)}{\Gamma(a)}. \tag{39}$$

The numerator is the incomplete Gamma function and the denominator is the Gamma function. Also, the pdf of X in (34) can be approximated as $f_X(x) \approx \text{InvGamma}\left(a, b^{-1}\right)$.

Since $\gamma = \rho MN/X$, the SINR pdf can be approximated as a Gamma pdf with shape parameter a and scale parameter ρMNb as

$$f_\gamma(\gamma) \approx \frac{1}{\Gamma(a)(q^{-1}b)^a}\gamma^{a-1}\exp\left(-\frac{\gamma}{q^{-1}b}\right). \tag{40}$$

Recall that $q = \frac{1}{\rho MN}$. The BER of ZF OTFS receiver for $\mathcal{M}$-QAM constellation, by using (40) and (16), is given as

$$P_{\text{ZF}} \approx \int_0^\infty C_{\mathcal{M}} \sum_{k=1}^{\log_2\sqrt{\mathcal{M}}} \sum_{i=0}^{(1-2^{-k})\sqrt{\mathcal{M}}-1} \Psi(i,k) Q\left(\sqrt{c\gamma}\right) \times \frac{1}{\Gamma(a)(q^{-1}b)^a}\gamma^{a-1}\exp\left(-\frac{\gamma}{q^{-1}b}\right)d\gamma,$$

where the constant $c = \frac{3(2i+1)^2}{\mathcal{M}-1}$. Using the relation $Q\left(\sqrt{c\gamma}\right) = \frac{1}{\sqrt{2\pi}}\int_{\sqrt{c\gamma}}^\infty e^{-t^2/2}dt$, the above expression can be simplified as follows

$$P_{\text{ZF}} \approx \int_0^\infty C_{\mathcal{M}} \sum_{k=1}^{\log_2\sqrt{\mathcal{M}}} \sum_{i=0}^{(1-2^{-k})\sqrt{\mathcal{M}}-1} \Psi(i,k) \times \frac{1}{\Gamma(a)(q^{-1}b)^a}\gamma^{a-1}\exp\left(-\frac{\gamma}{q^{-1}b}\right)\frac{1}{\sqrt{2\pi}}\int_{\sqrt{c\gamma}}^\infty e^{-t^2/2}dtd\gamma.$$

$$\begin{aligned} P_{\text{ZF}} &= \frac{\Delta}{2\pi}\sum_{k=0}^{K}\int_0^\infty \text{erfc}\left(\frac{1}{\sqrt{2qx}}\right)\text{Re}\left(\left\{\cos(u_k x) - i\sin(u_k x)\right\}\left\{\Phi_{\text{R}}(u_k) + i\Phi_{\text{I}}(u_k)\right\}\right)dx \\ &= \frac{\Delta}{2\pi}\sum_{k=0}^{K}\left\{\Phi_{\text{R}}(u_k)\int_0^\infty \text{erfc}\left(\frac{1}{\sqrt{2qx}}\right)\cos(u_k x)dx + \Phi_{\text{I}}(u_k)\int_0^\infty \text{erfc}\left(\frac{1}{\sqrt{2qx}}\right)\sin(u_k x)dx\right\} \\ &= \frac{\Delta}{2\pi}\sum_{k=0}^{K}\left\{\left(\Phi_{\text{R}}(u_k)\,\text{I}_1\right) + \left(\Phi_{\text{I}}(u_k)\,\text{I}_2\right)\right\}. \end{aligned} \tag{38}$$

By changing the order of integration, the above expression is rewritten as

$$P_{\text{ZF}} \approx C_{\mathcal{M}} \sum_{k=1}^{\log_2 \sqrt{\mathcal{M}}} \sum_{i=0}^{(1-2^{-k})\sqrt{\mathcal{M}}-1} \Psi(i,k) \frac{1}{\Gamma(a)(q^{-1}b)^a} \times \frac{1}{\sqrt{2\pi}} \int_0^{\infty} e^{-t^2/2} \int_0^{t^2/c} e^{-\frac{\gamma}{q^{-1}b}} \gamma^{a-1} d\gamma dt. \quad (41)$$

By substituting $\frac{\gamma}{q^{-1}b} = x$ above, we get

$$P_{\text{ZF}} \approx C_{\mathcal{M}} \sum_{k=1}^{\log_2 \sqrt{\mathcal{M}}} \sum_{i=0}^{(1-2^{-k})\sqrt{\mathcal{M}}-1} \Psi(i,k) \times \frac{1}{\Gamma(a)} \frac{1}{\sqrt{2\pi}} \int_0^{\infty} e^{-t^2/2} \int_0^{\frac{t^2}{cq^{-1}b}} e^{-x} x^{a-1} dx dt. \quad (42)$$

It is shown in [45, pp. 220] that

$$\int_0^z x^{a-1} e^{-x} dx = a^{-1} z^a e^{-z} {}_1F_1(1; a+1; z), \quad (43)$$

where ${}_1F_1(\cdot)$ is the confluent hypergeometric function. Using this property, (42) becomes

$$P_{\text{ZF}} \approx C_{\mathcal{M}} \sum_{k=1}^{\log_2 \sqrt{\mathcal{M}}} \sum_{i=0}^{(1-2^{-k})\sqrt{\mathcal{M}}-1} \Psi(i,k) \times \frac{1}{\Gamma(a+1)(cq^{-1}b)^a} \times \frac{1}{\sqrt{2\pi}} \int_0^{\infty} t^{2a} e^{-t^2\left(\frac{1}{cq^{-1}b}+\frac{1}{2}\right)} {}_1F_1\left(1; a+1; \frac{t^2}{cq^{-1}b}\right) dt. \quad (44)$$

We simplify (44) by substituting $\left(\frac{1}{cq^{-1}b} + \frac{1}{2}\right) = \alpha$ and $\alpha t^2 = y$ as

$$P_{\text{ZF}} \approx C_{\mathcal{M}} \sum_{k=1}^{\log_2 \sqrt{\mathcal{M}}} \sum_{i=0}^{(1-2^{-k})\sqrt{\mathcal{M}}-1} \frac{\Psi(i,k)}{2} \times \frac{1}{\Gamma(a+1)(cq^{-1}b)^a} \times \frac{1}{\sqrt{2\pi}} \left(\frac{1}{\alpha}\right)^{a+\frac{1}{2}} \int_0^{\infty} y^{a-\frac{1}{2}} e^{-y} {}_1F_1 \times \left(1; a+1; \frac{y}{cq^{-1}b\alpha}\right) dy. \quad (45)$$

Using the result

$$\Gamma(\sigma) {}_2F_1(\sigma, p; q; w) = \int_0^{\infty} e^{-y} y^{\sigma-1} {}_1F_1(p; q; wy) dy$$

from [45, pp. 59] in the above expression, we get the expression as in (46), as shown at the bottom of the next page. By replacing $\alpha = \left(\frac{1}{cq^{-1}b} + \frac{1}{2}\right)$ in (46), the BER expression is obtained as in (47), as shown at the bottom of the next page, where ${}_2F_1(\cdot)$ represents the Hypergeometric function. For 4-QAM, the BER expression in (47) can be simplified as follows:

$$P_{\text{ZF}_{\text{QPSK}}} \approx \frac{\sqrt{q^{-1}b/2\pi}}{2\left(1+\frac{q^{-1}b}{2}\right)^{a+\frac{1}{2}}} \frac{\Gamma\left(a+\frac{1}{2}\right)}{\Gamma(a+1)} \times {}_2F_1\left(1, a+\frac{1}{2}; a+1; \frac{1}{1+\frac{q^{-1}b}{2}}\right). \quad (48)$$

This section derived the BER of OTFS ZF receivers with perfect receive CSI. We will show later in Section-IV that the theoretical BER expressions match their numerical counterparts. We see that the above BER expression is radically different from that of the ZF receiver in conventional [34, Eq. (13)] [35, Eq. (32)]. This is because the SINR pdf in [30], [35], unlike the current work, has a weighted Chi-Square distribution. We next derive the BER expression with imperfect receive CSI. Before doing that, a remark is in order.

Remark 4: The proposed ideas can be extended for deriving the BER of MMSE receiver, but the extension would definitely be non-trivial. Similar to the current work, the SINR derivation, depending on whether the matrix $\mathbf{H}^H\mathbf{H} + \rho\mathbf{I}$ has one/two/n distinct eigenvalues, can be divided into three cases. The challenges imposed by the addition of $\rho\mathbf{I}$ to matrix $\mathbf{H}^H\mathbf{H}$ in deriving the SINR pdf for the MMSE receiver will have to be handled. Further, the relatively complicated MMSE SINR expression, while deriving the SINR pdf, will pose additional challenges. One may again exploit the doubly circulant structure of $\mathbf{H}$ to tackle these challenges.

B. SINR and BER Calculation With Imperfect Receive CSI

We now extend the earlier BER derivation for the case when the receiver has imperfect receive CSI. We show that the SINR for this case, which is denoted as $\hat{\gamma}$, is a scaled function of γ. The earlier BER expressions can then be easily extended to the imperfect receive CSI. To achieve this aim, we begin by modeling the estimate of $\mathbf{H}$ as follows [30]: $\widehat{\mathbf{H}} = \mathbf{H} + \mathbf{\Delta H}$. The channel estimation error matrix $\mathbf{\Delta H}$ satisfies the following properties [30]

- It is independent of $\mathbf{H}$, and its non-zero elements in a row/column are i.i.d. with pdf $\mathcal{CN}(0, \sigma_e^2)$ [30]. The variance σ_e^2 captures the channel estimator accuracy [30].
- It, similar to $\mathbf{H}$, is also a doubly circulant matrix[2] [20].

The channel estimate $\widehat{\mathbf{H}}$, consequently, is also a doubly circulant matrix. The ZF data vector estimate with imperfect receive CSI can now be obtained from (6) as follows

$$\widehat{\mathbf{x}} = \widehat{\mathbf{H}}^{\dagger}(\mathbf{H}\mathbf{x} + \mathbf{v}) = (\mathbf{H} + \mathbf{\Delta H})^{\dagger}(\mathbf{H}\mathbf{x} + \mathbf{v}). \quad (49)$$

[2]A channel estimation algorithm estimates locations and gains of delay-Doppler channel paths, and then reconstructs the estimated channel matrix $\widehat{\mathbf{H}}$ by substituting the gains at the estimated non-zero locations [46], [47]. Since an efficient estimation algorithm correctly estimates the delay-Doppler locations with a high probability [47, Fig. 4(a)], the reconstructed physical channel $\widehat{\mathbf{H}}$ will also have a doubly block-circulant structure. The physical error matrix $\Delta\mathbf{H} = \widehat{\mathbf{H}} - \mathbf{H}$ will have a doubly circulant structure. Due to the aforementioned reasons, the channel estimation literature commonly assumes that the channel estimation matrix also has the same structure as that of the original one [20], [30], which we also do in the current work.

The magnitude of $\mathbf{\Delta H}$ entries is typically smaller than $\mathbf{H}$ [37]. The matrix $\widehat{\mathbf{H}}^{\dagger}$ can be well approximated using the first order Taylor series expansion as follows [37]:

$$\widehat{\mathbf{H}}^{\dagger} = (\mathbf{H} + \mathbf{\Delta H})^{\dagger} \approx \mathbf{H}^{\dagger} \left(\mathbf{I}_{MN} - \mathbf{\Delta H} \mathbf{H}^{\dagger} \right). \tag{50}$$

Equation (49) is therefore re-expressed as

$$\widehat{\mathbf{x}} = \left(\mathbf{H}^{\dagger} - \mathbf{H}^{\dagger} \mathbf{\Delta H} \mathbf{H}^{\dagger} \right) (\mathbf{H}\mathbf{x} + \mathbf{v}) = \mathbf{x} + \mathbf{w}. \tag{51}$$

The vector $\mathbf{w} = \mathbf{H}^{\dagger}\mathbf{v} - \mathbf{H}^{\dagger}\mathbf{\Delta H}\mathbf{x} - \mathbf{H}^{\dagger}\mathbf{\Delta H}\mathbf{H}^{\dagger}\mathbf{v}$ denotes the noise plus interference due to channel estimation error. Since $\mathbf{\Delta H}$ is a doubly circulant matrix, we decompose it, similar to (9), as $\mathbf{\Delta H} = \mathbf{\Psi}^{H} \mathbf{\Delta D} \mathbf{\Psi}$. The diagonal matrix $\mathbf{\Delta D} \in \mathbb{C}^{MN \times MN}$ consists of eigenvalues of $\mathbf{\Delta H}$. The noise plus interference vector $\mathbf{w}$ can consequently be expressed as

$$\mathbf{w} = \mathbf{\Psi}^{H}\mathbf{D}^{\dagger}\mathbf{\Psi}\mathbf{v} - \mathbf{\Psi}^{H}\mathbf{D}^{\dagger}\mathbf{\Delta D}\mathbf{\Psi}\mathbf{x} - \mathbf{\Psi}^{H}\mathbf{D}^{\dagger}\mathbf{\Delta D}\mathbf{D}^{\dagger}\mathbf{\Psi}\mathbf{v}. \tag{52}$$

Recall that the non-zero elements in a row/column of $\mathbf{\Delta H}$ are i.i.d. with pdf $\mathcal{CN}(0, \sigma_e^2)$. It follows from Appendix B that each diagonal element of $\mathbf{\Delta D}$ has pdf $\mathcal{CN}(0, \sigma_\epsilon^2)$ with $\sigma_\epsilon^2 = \sigma_e^2 P$.The SINR of the kth symbol of the estimate $\widehat{\mathbf{x}}$ with imperfect receive CSI, using (51), is therefore given as

$$\hat{\gamma}_k = \frac{P_x}{[\mathbf{G}]_{k,k}}, \quad \text{for} \;\; 1 \le k \le MN. \tag{53}$$

Here $\mathbf{G} = \mathbb{E}[\mathbf{w}\mathbf{w}^{H}]$ is the covariance matrix of the vector $\mathbf{w}$. We now state the following *Lemma* whose proof is relegated to Appendix F

Lemma 5: The SINR $\hat{\gamma}$ can be derived by scaling the perfect receive CSI SINR γ as

$$\hat{\gamma} = \frac{1}{1 + \sigma_\epsilon^2 \rho} \gamma. \tag{54}$$

We have dropped the subscript k since, as shown in Appendix F, the SINR $\hat{\gamma}$ of each estimated symbol has identical statistical characteristics. Let $f_{\hat{\gamma}}(\hat{\gamma})$ be the pdf of SINR $\hat{\gamma}$. The ZF receiver BER for OTFS systems with imperfect receive CSI can be derived using (14) as $\hat{P}_{\text{ZF}} = \int_0^{\infty} P_b f_{\hat{\gamma}}(\hat{\gamma}) d\hat{\gamma}$. We see from *Lemma*-5 that the pdf $f_{\hat{\gamma}}(\hat{\gamma})$ can be calculated directly by using the pdf $f_{\gamma}(\gamma)$ derived in Section-III-A for the different cases. Consequently, depending on the delay-Doppler locations, similar to the perfect receive CSI case in Section-III-A, we have the following cases for imperfect CSI.

1) All Eigenvalues of $\mathbf{H}^{H}\mathbf{H}$ Are Identical: The SINR can be derived using (54) as

$$\hat{\gamma} = \frac{\rho MN}{(1 + \sigma_\epsilon^2 \rho) \frac{MN}{|\lambda|^2}} = \frac{\rho}{(1 + \sigma_\epsilon^2 \rho)} \phi. \tag{55}$$

Here $\phi = |\lambda|^2 \sim \text{Exp}(1/\sigma^2)$, which implies that $f_{\hat{\gamma}}(\hat{\gamma}) = \frac{1+\sigma_\epsilon^2\rho}{\rho\sigma^2} \exp\left(-\frac{1+\sigma_\epsilon^2\rho}{\rho\sigma^2} \hat{\gamma} \right)$. The BER expression, similar to Section-III-A.1, is derived as

$$P_{\text{ZF}} = C_{\mathcal{M}} \sum_{k=1}^{\log_2 \sqrt{\mathcal{M}}} \sum_{i=0}^{(1-2^{-k})\sqrt{\mathcal{M}}-1} \frac{\Psi(i,k)}{2} \times \left[1 - \sqrt{\frac{(2i+1)^2 3\rho\sigma^2}{2(\mathcal{M}-1)(1+\sigma_\epsilon^2\rho) + (2i+1)^2 3\rho\sigma^2}} \right].$$

For 4-QAM, the above BER expression simplifies as

$$P_{\text{ZF}_{\text{QPSK}}} = \frac{1}{2} \left[1 - \sqrt{\frac{\rho\sigma^2}{2(1+\sigma_\epsilon^2\rho) + \rho\sigma^2}} \right]. \tag{56}$$

2) $\mathbf{H}^{H}\mathbf{H}$ Has Two Distinct Eigenvalues: The SINR for this case is obtained from (54) using the steps given in Section-III-A.2 as

$$\hat{\gamma} = \frac{\rho MN}{(1+\sigma_\epsilon^2\rho)\frac{MN}{2}\left(\frac{1}{|\lambda_1|^2} + \frac{1}{|\lambda_2|^2}\right)} = \frac{2\rho}{(1+\sigma_\epsilon^2\rho)} \underbrace{\frac{|\lambda_1|^2|\lambda_2|^2}{|\lambda_1|^2 + |\lambda_2|^2}}_{\phi}. \tag{57}$$

Here the pdf of ϕ is $f_{\phi}(\phi) = \frac{1}{\sigma^2} \text{E}_1\left(\frac{\phi}{\sigma^2}\right)$, and therefore $f_{\hat{\gamma}}(\hat{\gamma}) = \frac{(1+\sigma_\epsilon^2\rho)}{2\rho\sigma^2} \text{E}_1\left(\frac{(1+\sigma_\epsilon^2\rho)}{2\rho\sigma^2}\hat{\gamma}\right)$. The BER expression, similar to Section-III-A.2, can now be derived as in (58), as shown at the bottom of the next page, where the parameters $a = \frac{(1+\sigma_\epsilon^2\rho)}{2\rho\sigma^2}$ and $b = \frac{(2i+1)^2 3}{2(\mathcal{M}-1)}$. For $\mathcal{M} = 4$, the BER expression is given in (59), as shown at the bottom of the next page.

3) $\mathbf{H}^{H}\mathbf{H}$ Has n Distinct Eigenvalues: The matrix $\mathbf{D}^{H}\mathbf{D}$ now has n distinct $|\lambda_i|^2$s. We derive the SINR, similar to Section-III-A.3, using (54) as

$$\hat{\gamma} = \frac{\rho MN}{(1+\sigma_\epsilon^2\rho) \sum_{i=1}^{n} \frac{C_i}{|\lambda_i|^2}}. \tag{60}$$

Using the steps explained in Section-III-A.3, we obtain the BER formula as given in (61), as shown at the bottom of the next page, where ${}_2F_1(\cdot)$ denotes the Hypergeometric function.

$$P_{\text{ZF}} \approx C_{\mathcal{M}} \sum_{k=1}^{\log_2 \sqrt{\mathcal{M}}} \sum_{i=0}^{(1-2^{-k})\sqrt{\mathcal{M}}-1} \frac{\Psi(i,k)}{2} \frac{1}{\Gamma(a+1)(cq^{-1}b)^a} \frac{1}{\sqrt{2\pi}} \left(\frac{1}{\alpha}\right)^{a+\frac{1}{2}} \Gamma\left(a+\frac{1}{2}\right) {}_2F_1\left(\left(a+\frac{1}{2}\right), 1; a+1; \frac{1}{cq^{-1}b\alpha}\right) \tag{46}$$

$$P_{\text{ZF}} \approx C_{\mathcal{M}} \sum_{k=1}^{\log_2 \sqrt{\mathcal{M}}} \sum_{i=0}^{(1-2^{-k})\sqrt{\mathcal{M}}-1} \Psi(i,k) \frac{\sqrt{cq^{-1}b/2\pi}}{2\left(1 + \frac{cq^{-1}b}{2}\right)^{a+\frac{1}{2}}} \frac{\Gamma\left(a+\frac{1}{2}\right)}{\Gamma(a+1)} \times {}_2F_1\left(1, \left(a+\frac{1}{2}\right); a+1; \frac{1}{1+\frac{cq^{-1}b}{2}}\right) \tag{47}$$

TABLE II
CHANNEL PARAMETERS

Channel tap no.	1	2	3	4	5	6	7	8	9
Delay (ns)	0	30	150	310	370	710	1090	1730	2510
Relative Power (dB)	0	-1.5	-1.4	-3.6	-0.6	-9.1	-7.0	-12.0	-16.9

The shape parameter a and the rate b in (62) are obtained by fitting the CDF of random variable X in (31) in Gamma CDF, and the parameters $c = \frac{3(2i+1)^2}{(\mathcal{M}-1)}$ and $\hat{q} = (1+\sigma_\epsilon^2\rho)q$. The BER expression in (61) for $\mathcal{M} = 4$, is simplified as

$$P_{\text{ZF}_{\text{QPSK}}} \approx \frac{\sqrt{\hat{q}^{-1}b/2\pi}}{2\left(1+\frac{\hat{q}^{-1}b}{2}\right)^{a+\frac{1}{2}}}\frac{\Gamma\left(a+\frac{1}{2}\right)}{\Gamma\left(a+1\right)} \times {}_2F_1\left(1, a+\frac{1}{2}; a+1; \frac{1}{1+\frac{\hat{q}^{-1}b}{2}}\right). \quad (62)$$

Here $\sigma_\epsilon^2 = P\sigma_e^2$ with σ_e^2 being channel estimation error variance. We see that with imperfect receive CSI also, the derived BER expressions are significantly different from that of the conventional MIMO systems in [30, Eq. (22)] [31, Eq. (25)]. This is because the SINR pdf in [30], [31], contrary to the current work, has a Chi-square distribution.

IV. SIMULATION RESULTS

We now compare the BER provided by theoretical expressions derived in this work with the one provided by numerically simulating an OTFS system. For the studies in this section, we consider an OTFS system with a subcarrier spacing of $\Delta f = 15$ KHz and a carrier frequency of 4 GHz. The maximum Doppler shift, similar to the OTFS works in [7], [9], [11], [14], [47] is set as $\nu_{\max} = 1851$ Hz, which corresponds to a speed of 500 Km/h. We also select, similar to [9], [11], [14], the delay profile from the extended vehicular A (EVA) model [48], as shown in Table II. We generate the Doppler values using the Jake's formula $\nu_i = \nu_{\max}\cos(\theta_i)$ with θ_i distributed uniformly in the range $[-\pi, \pi]$ [9], [47]. We also consider, similar to exiting OTFS studies [11], [13], the number of propagation paths L_h in the range $1 \leq L_h \leq 9$. It is worthwhile noting that reference [13] and [11] considered $L_h = 4$, and $L_h = 9$, respectively. The delay and Doppler taps l_i and k_i for the ith propagation path are in the range $0 < l_i \leq l_{max}$ and $0 < k_i \leq k_{max}$, where $l_{max} < M-1$ and $k_{max} < N-1$ are the integer delay and Doppler taps corresponding to the maximum delay τ_{max} and Doppler ν_{max}. We define the SNR, similar to [13], as $\rho = P_x/\sigma_v^2$. We divide the numerical investigations into perfect CSI (PCSI) and imperfect CSI (ICSI) scenarios. Within each scenario, we consider the following three cases.

- **Case A:** matrix $\mathbf{H}^H\mathbf{H}$ has only one distinct eigenvalue. This implies that the diagonal matrix $\mathbf{D}^H\mathbf{D}$ has identical entries:$|\lambda_1|^2 = |\lambda_2|^2 = \ldots = |\lambda_{MN}|^2 = |\lambda|^2$.
- **Case B:** matrix $\mathbf{H}^H\mathbf{H}$ has only two distinct independent eigenvalues. The diagonal matrix $\mathbf{D}^H\mathbf{D}$, consequently, has two distinct entries: $|\lambda_1|^2 = |\lambda_3|^2 = \ldots = |\lambda_{MN-1}|^2 = |\lambda_1|^2$ and $|\lambda_2|^2 = |\lambda_4|^2 = \ldots = |\lambda_{MN}|^2 = |\lambda_2|^2$.
- **Case C:** $\mathbf{H}^H\mathbf{H}$ has n distinct eigenvalues, which implies that $\mathbf{D}^H\mathbf{D}$ has n distinct $|\lambda_i|^2$.

A. Perfect Receive CSI

We begin by showing the effectiveness of the ZF receiver for OTFS systems. Fig. 2 (a) compares the BER of the ZF and MP receivers for OTFS with BPSK modulation and perfect CSI. The *non-linear* MP receiver outperforms the *linear* ZF receiver. This is because the *computationally-complex non-linear* MP receiver provides an approximate ML solution. For a fair comparison with the non-linear MP receiver, we also plot the BER of ZF-LAS receiver wherein the ZF receiver is followed by low-complexity local-search-based non-linear likelihood ascent search (LAS) operation. The LAS receiver begins with an initial solution provided by the ZF receiver, and searches for good solutions in the neighborhood until a local optimum is reached [49]. We see that the BER gap between ZF-LAS and the MP receiver has reduced significantly. As shown in [20], the complexity order of the ZF-LAS receiver is same as that of the ZF receiver. *This gap could be further bridged by using another low-complexity non-linear*

$$P_{\text{ZF}} = C_{\mathcal{M}}\left[\frac{1}{2} - \frac{(1+\sigma_\epsilon^2\rho)}{4\rho\sigma^2}\left\{\frac{1}{a}\left(1+\frac{a}{b}\right)^{\frac{1}{2}} + \frac{1}{2b}\ln\left(\frac{\sqrt{a+b}-\sqrt{b}}{\sqrt{a+b}+\sqrt{b}}\right)\right\}\right]\sum_{k=1}^{\log_2\sqrt{\mathcal{M}}}\sum_{i=0}^{(1-2^{-k})\sqrt{\mathcal{M}}-1}\Psi(i,k), \quad (58)$$

$$P_{\text{ZF}_{\text{QPSK}}} = \frac{1}{2}\left[1 - \left\{\left(1+\frac{(1+\sigma_\epsilon^2\rho)}{\rho\sigma_2^2}\right)^{\frac{1}{2}} + \frac{(1+\sigma_\epsilon^2\rho)}{2\rho\sigma_2^2}\ln\left(\frac{\sqrt{(1+\sigma_\epsilon^2\rho)+\rho\sigma_2^2}-\sqrt{\rho\sigma_2^2}}{\sqrt{(1+\sigma_\epsilon^2\rho)+\rho\sigma_2^2}+\sqrt{\rho\sigma_2^2}}\right)\right\}\right]. \quad (59)$$

$$P_{\text{ZF}} \approx C_{\mathcal{M}}\sum_{k=1}^{\log_2\sqrt{\mathcal{M}}}\sum_{i=0}^{(1-2^{-k})\sqrt{\mathcal{M}}-1}\Psi(i,k)\frac{\sqrt{c\hat{q}^{-1}b/2\pi}}{2\left(1+\frac{c\hat{q}^{-1}b}{2}\right)^{a+\frac{1}{2}}}\frac{\Gamma\left(a+\frac{1}{2}\right)}{\Gamma\left(a+1\right)}{}_2F_1\left(1, a+\frac{1}{2}; a+1; \frac{1}{1+\frac{c\hat{q}^{-1}b}{2}}\right). \quad (61)$$

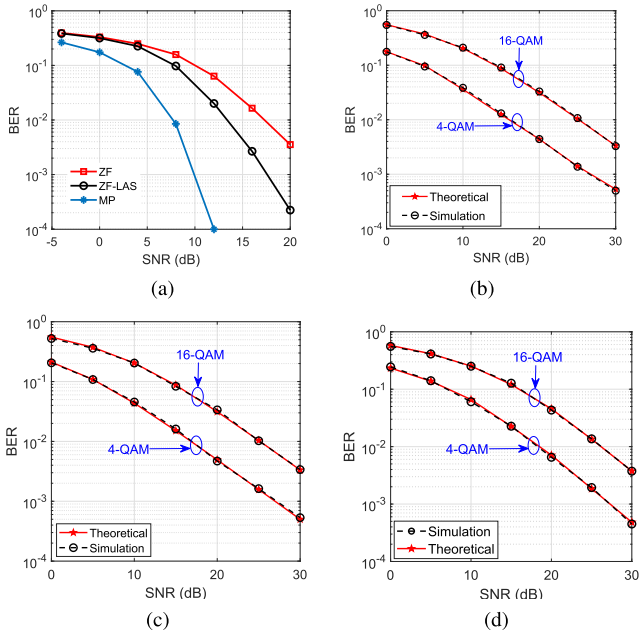

Fig. 2. (a) BER comparison of the ZF, with and without LAS technique, and MP receiver for OTFS systems with $M = N = 32$, BPSK, and perfect CSI. Comparison of theoretical and numerical BER for Case A with perfect CSI: (b) $M = N = 16, L_h = 1$; and (c) $M = N = 32, L_h = 1$. Comparison of theoretical and numerical BER for Case B with perfect CSI: (d) $M = 16, N = 2, L_h = 2$.

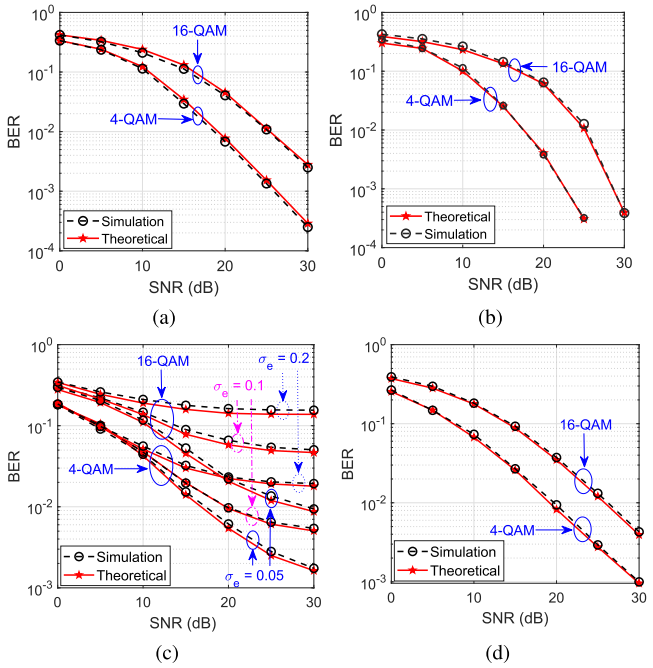

Fig. 3. Comparison of theoretical and numerical BER with perfect CSI for Case C: (a) $M = N = 16, L_h = 4$; and (b) $M = N = 32, L_h = 9$. With imperfect CSI for Case A with $M = N = 16$ and $L_h = 1$: (c) σ_e^2 is independent of the SNR; and (d) $\sigma_e^2 = 1/\rho$.

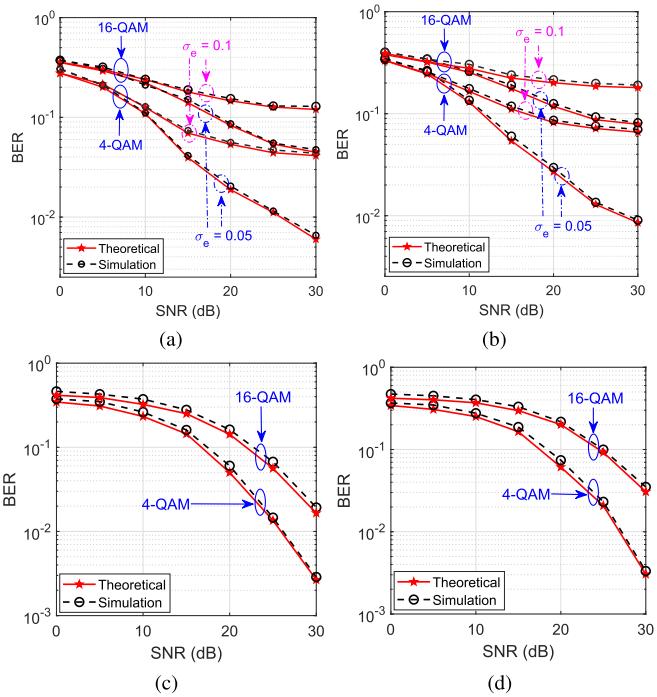

Fig. 4. Comparison of simulated and theoretical BER for Case C with imperfect CSI. For (a) and (c) $M = N = 16, L_h = 4$, and for (b) and (d) $M = N = 32, L_h = 5$. For the first two figures, channel estimation error variance σ_e^2 is independent of SNR ρ. For the last two, $\sigma_e^2 = 1/\rho$.

technique better than LAS, whose investigation is a direction of future research.

We now plot in Fig. 2(b) and Fig. 2(c), the BER calculated using the derived theoretical expression for Case A for $\{4, 16\}$-QAM constellations. We compare this BER with the one obtained by numerically simulating an OTFS system. For Fig. 2(b), the number of delay bins M and the Doppler bins N are set as $M = N = 16$. For Fig. 2(c), $M = N = 32$. For both these figures, the number of channel path $L_h = 1$. We observe that the theoretical and numerical results match for both QAM constellations. This demonstrates the efficacy of the derived BER expressions. We now compare in Fig. 2(d) the theoretical and numerical BER values for Case B with $M = 16$, $N = 2$, and $L_h = 2$. We choose delay-Doppler location of the propagation paths such that $\mathbf{D}^H\mathbf{D}$ has two independent distinct $|\lambda|_i^2$. We again observe that theoretical BER closely matches its numerical counterpart.

We now compare in Fig. 3(a) and Fig. 3(b) the theoretical and numerical BER for Case C. For Fig. 3(a), $M = N = 16$ and $L_h = 4$, and Fig. 3(b), $M = N = 32$ and $L_h = 9$. We see that for both 4- and 16-QAM constellations, and for different number of propagation paths, theoretical BER closely agrees with the numerical BER values. The negligible gaps between the theoretical and simulated BERs exist due to the SNR pdf approximation as Gamma, as explained in Section III-A.3, and also shown in Fig. 1.

B. Imperfect Receive CSI

We now validate the derived BER expressions for imperfect receive CSI by assuming $M = N = 16$, and $L_h = 1$. We plot the theoretical and numerical BER in i) Fig. 3 (c) for Case A when the channel estimation error variance σ_e^2, and consequently $\sigma_\epsilon^2 = \sigma_e^2 P$, is independent of SNR; and b) Fig. 3 (d) when σ_e^2 a function of SNR and vary it as $\sigma_e^2 = 1/\rho$, where $\rho = P_x/\sigma_v^2 =$ SNR. We observe from the two figures

that the theoretical and numerical BER plots match for both 4-and 16-QAM constellations. The BER floors in Fig. 3(c) at high SNR, as the channel estimate error dominates that of the noise. A negligible gap between the simulated and theoretical BER plots is due to the first order Taylor series approximation in (50).

We next validate the derived BER expressions with imperfect receive CSI for Case C, wherein $\mathbf{H}^H\mathbf{H}$ has n distinct eigenvalues. In Fig. 4(a) and Fig. 4(b), we fix the channel estimation error variance σ_e^2. For Fig. 4(a) we set the delay-Doppler bins as $M = N = 16$ and the number of delay-Doppler propagation paths $L_h = 4$. For Fig. 4(b) $M = N = 32$ and $L_h = 5$. We observe from these figures that for both 4-and 16-QAM constellations, and for different simulation parameters, the theoretical BER values closely follow their numerical BER counterparts. The negligible gap between the two is due to the CDF approximation in (39). We repeat the last study in Fig. 4(c) and Fig. 4(d) by varying σ_e^2 as $\sigma_e^2 = 1/\rho$. For Fig. 4(c), $M = N = 16$ and $L_h = 4$ and Fig. 4(d), $M = N = 32$ and $L_h = 5$. We see that the theoretical and numerical BER values again match. The negligible gap between them is due to the CDF approximation in (39).

V. Conclusion and Future Directions

We derive a closed form BER expression for the zero-forcing OTFS receiver by calculating the pdf of its SINR. We numerically showed that the BER calculated using this proposed closed form expression closely matches the one obtained numerically for different constellations and OTFS system parameters. The current work considered single-antenna OTFS system. The future directions of this work is to derive BER expression for ZF receiver for angular domain MIMO OTFS and massive MIMO OTFS systems by utilizing the SINR pdf expressions derived herein. Future works may also investigate BER of ZF based non-linear receiver for OTFS systems.

Appendix A

The channel matrix $\mathbf{H} = \texttt{CIRC}(\mathbf{A}_0, \mathbf{A}_1, \mathbf{A}_2, \ldots, \mathbf{A}_{M-1})$ is constructed as

$$\mathbf{H} = \begin{bmatrix} \mathbf{A}_0 & \mathbf{A}_1 & \cdots & \mathbf{A}_{M-2} & \mathbf{A}_{M-1} \\ \mathbf{A}_{M-1} & \mathbf{A}_0 & \ddots & \mathbf{A}_{M-3} & \mathbf{A}_{M-2} \\ \vdots & \ddots & \ddots & \ddots & \vdots \\ \mathbf{A}_2 & \mathbf{A}_3 & \ddots & \mathbf{A}_0 & \mathbf{A}_1 \\ \mathbf{A}_1 & \mathbf{A}_2 & \cdots & \mathbf{A}_{M-1} & \mathbf{A}_0 \end{bmatrix}. \tag{63}$$

The construction of $\mathbf{H}$ can be recast as [50]

$$\mathbf{H} = \sum_{i=0}^{M-1} \left(\mathbf{\Pi}_M^i \otimes \mathbf{A}_i\right). \tag{64}$$

Here $\mathbf{\Pi}_M = \text{CIRC}[0, 1, 0, \ldots, 0]$ is the $M \times M$ circulant permutation matrix. The circulant matrix $\mathbf{\Pi}_M^i$ can be diagonalized using the DFT matrix as follows $\mathbf{\Pi}_M^i = \mathbf{F}_M^H \mathbf{\Omega}_M^i \mathbf{F}_M$ [50], where the diagonal matrix $\mathbf{\Omega}_M^i = \text{diag}\left[1, W_M^i, W_M^{2i}, \ldots, W_M^{i(M-1)}\right]$ with $W_M = e^{j2\pi/M}$, and $\mathbf{F}_M$ is an $M \times M$ DFT matrix. By using this decomposition, we get

$$\mathbf{\Pi}_M^i \otimes \mathbf{A}_i = \left(\mathbf{F}_M^H \mathbf{\Omega}_M^i \mathbf{F}_M\right) \otimes \left(\mathbf{F}_N^H \mathbf{F}_N \mathbf{A}_i \mathbf{F}_N^H \mathbf{F}_N\right). \tag{65}$$

Since $\mathbf{A}_i$ is an $N \times N$ circulant matrix, it can also be similarly diagonalized using the DFT matrix $\mathbf{F}_N$ as $\mathbf{A}_i = \mathbf{F}_N^H \mathbf{D}_i \mathbf{F}_N$, where the diagonal matrix $\mathbf{D}_i$ consists of eigenvalues of the matrix $\mathbf{A}_i$. Substituting this decomposition in (65), we get

$$\begin{aligned} \mathbf{\Pi}_M^i \otimes \mathbf{A}_i &= \left(\mathbf{F}_M^H \mathbf{\Omega}_M^i \mathbf{F}_M\right) \otimes \left(\mathbf{F}_N^H \mathbf{D}_i \mathbf{F}_N\right) \\ &\overset{(a)}{=} \left(\mathbf{F}_M^H \otimes \mathbf{F}_N^H\right) \left(\mathbf{\Omega}_M^i \otimes \mathbf{D}_i\right) \left(\mathbf{F}_M \otimes \mathbf{F}_N\right). \end{aligned} \tag{66}$$

Equality (a) above is due to the identity $(\mathbf{A} \otimes \mathbf{B})(\mathbf{C} \otimes \mathbf{D}) = \mathbf{AC} \otimes \mathbf{BD}$ [50]. Substitution of (66) in (64) along with $\mathbf{D} = \sum_{i=0}^{M-1} \left(\mathbf{\Omega}_M^i \otimes \mathbf{D}_i\right)$ yield the desired result in (7). By expanding the Kronecker product in $\mathbf{D} = \sum_{i=0}^{M-1} \left(\mathbf{\Omega}_M^i \otimes \mathbf{D}_i\right)$, we get the expression of $\mathbf{D}$ in (8).

Appendix B

The matrix $\mathbf{D} \in \mathbb{C}^{MN \times MN}$ in (8) can be written as [11]:

$$\mathbf{D} = \sum_{i=0}^{M-1} \mathbf{\Omega}_M^i \otimes \mathbf{D}_i. \tag{67}$$

Here $\mathbf{D}_i \in \mathbb{C}^{N \times N}$ consists of the eigenvalues of the ith $N \times N$ circulant block of the channel matrix $\mathbf{H}$. A circulant matrix $\mathbf{C}$ can be diagonalized using a DFT matrix [51]. Its eigenvalues can therefore be calculated by taking the DFT of its first column [51]. We thus have $\mathbf{D}_i = \text{diag}[\bar{\mathbf{F}}_N \mathbf{H}_i(:, 1)]$, where $\bar{\mathbf{F}}_N \in \mathbb{C}^{N \times N}$ is the DFT matrix and $\mathbf{H}_i(:, 1) \in \mathbb{C}^{N \times 1}$ is the first column of the ith circulant block of $\mathbf{H}$. Using this property, the lth diagonal entry of $\mathbf{D}_i$ is

$$\lambda_l^i = \sum_{n=0}^{N-1} h_n^i \exp\{-j2\pi ln/N\}, \tag{68}$$

where h_n^i denotes the nth entry of the first column in the ith circulant block of $\mathbf{H}$. Let L_h^i be the number of non-zero entries in a column or row of the ith circulant block of $\mathbf{H}$. Also $\sum_{i=1}^{M} L_h^i = L_h$ be the number of non-zero entries per row in $\mathbf{H}$, which is the number of delay-Doppler propagation paths. Since these non-zero entries are i.i.d. with pdf $\mathcal{CN}(0, \frac{1}{L_h})$, we see that λ_l^i also has a complex Gaussian pdf with mean $\mathbb{E}[\lambda_l^i] = 0$ and variance $\mathbb{E}\left[|\lambda_l^i|^2\right] = \frac{L_h^i}{L_h}$. Each diagonal entry of $\mathbf{D}_i$ is therefore distributed as $\mathcal{CN}(0, \frac{L_h^i}{L_h})$. Since $\mathbf{\Omega}_M^i = \text{diag}[1, e^{j2\pi i/M}, e^{j4\pi i/M}, \ldots, e^{j2\pi i(M-1)/M}]$, it readily follows from (67) that each diagonal element of the eigenvalue matrix $\mathbf{D}$ also has a complex Gaussian pdf with mean zero and variance $\frac{1}{L_h} \sum_{i=1}^{M} L_h^i$.

Appendix C

The probability of error for this case, using (16), is given as $P_{\text{ZF}} = \int_0^\infty P_b \frac{1}{\rho\sigma_i^2} \exp(-\frac{\gamma}{\rho\sigma^2}) d\gamma$. Substituting P_b from (14), we get P_{ZF} as expressed as shown at the bottom of the next page in (69), where we have also used the Craig's formula [52] to replace $Q(x)$ as

$$Q(x) = \frac{1}{\pi} \int_0^{\frac{\pi}{2}} \exp\left(-\frac{x^2}{2\sin^2\theta}\right) d\theta. \tag{70}$$

After integrating (69) with respect to γ, we get

$$P_{\text{ZF}} = \frac{1}{\pi}\int_0^{\frac{\pi}{2}} C_{\mathcal{M}} \sum_{k=1}^{\log_2\sqrt{\mathcal{M}}} \sum_{i=0}^{(1-2^{-k})\sqrt{\mathcal{M}}-1} \Psi(i,k) \times \frac{\sin^2\theta}{\sin^2\theta + \frac{(2i+1)^2 3\rho\sigma^2}{2(\mathcal{M}-1)}} d\theta. \quad (71)$$

It follows from [53, pp. 125] that

$$\frac{1}{\pi}\int_0^{\frac{\pi}{2}} \left(\frac{\sin^2\theta}{\sin^2\theta + c^2}\right)^m = \frac{1}{2}\left[1 - \mu_c \sum_{k=0}^{m-1} \binom{2k}{k}\left(\frac{1-\mu_c^2}{4}\right)\right],$$

where $\mu_c \triangleq \sqrt{\frac{c}{1+c}}$. With $m = 1$ and $c = \frac{(2i+1)^2 3\rho\sigma^2}{2(\mathcal{M}-1)}$, the above integration reduces to

$$\frac{1}{2}\left[1 - \sqrt{\frac{(2i+1)^2 3\rho\sigma^2}{2(\mathcal{M}-1) + (2i+1)^2 3\rho\sigma^2}}\right]. \quad (72)$$

The BER expression in (20) can now be obtained by substituting the above expression in (71).

APPENDIX D

By substituting (27) in (16), the BER of the ZF receiver for $\mathcal{M}$-QAM is given as

$$P_{\text{ZF}} = \int_0^{\infty} C_{\mathcal{M}} \sum_{k=1}^{\log_2\sqrt{\mathcal{M}}} \sum_{i=0}^{(1-2^{-k})\sqrt{\mathcal{M}}-1} \frac{\Psi(i,k)}{2\rho\sigma^2} \times Q\left((2i+1)\sqrt{\frac{3\gamma}{\mathcal{M}-1}}\right) \text{E}_1\left(\frac{\gamma}{2\rho\sigma^2}\right) d\gamma.$$

By expressing the Q-function in terms of error function as $Q(x) = \frac{1}{2}\text{erfc}\left(\frac{x}{\sqrt{2}}\right)$, the above BER expression can be equivalently expressed as

$$P_{\text{ZF}} = \int_0^{\infty} C_{\mathcal{M}} \sum_{k=1}^{\log_2\sqrt{\mathcal{M}}} \sum_{i=0}^{(1-2^{-k})\sqrt{\mathcal{M}}-1} \frac{\Psi(i,k)}{4\rho\sigma^2} \times \text{erfc}\left((2i+1)\sqrt{\frac{3\gamma}{2(\mathcal{M}-1)}}\right) \text{E}_1\left(\frac{\gamma}{2\rho\sigma^2}\right) d\gamma. \quad (73)$$

Using $\int_0^{\infty} \text{E}_1(ax)dx = \frac{1}{a}$, and the property [41, pp. 5.18]

$$\int_0^{\infty} \text{erf}(\sqrt{bx})\text{E}_1(ax)dx = \frac{1}{a}\left(1+\frac{a}{b}\right)^{1/2} + \frac{1}{2b}\ln\left(\frac{\sqrt{a+b}-\sqrt{b}}{\sqrt{a+b}+\sqrt{b}}\right),$$

the desired result in *Lemma*-4 can now be obtained by solving the integral in (73).

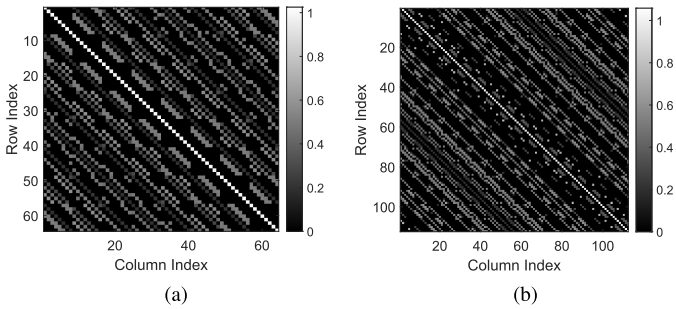

Fig. 5. Absolute values of correlation matrix of the vector diag $\left[\mathbf{D}^H\mathbf{D}\right]$: (a) $M = N = 8, L_h = 5$; and (b) $M = 16, N = 7, L_h = 5$. Delay-Doppler location of the propagation path are chosen randomly.

APPENDIX E

Let $X_i = C_i|\lambda_i|^{-2}$ be the ith weighted inverted Gamma random variable in (32) such that $X = \sum_{i=1}^{n} X_i$. It follows from Appendix B that $X_i \sim \text{InvGamma}(1, C_i/\sigma_i^2)$ since $\lambda_i \sim \mathcal{CN}(0, \sigma_i^2)$. The pdf of X_i is therefore given as

$$f_{X_i}(x_i) = \frac{C_i}{\sigma_i^2} x_i^{-2} \exp\left\{-\frac{C_i}{\sigma_i^2 x_i}\right\}. \quad (74)$$

The characteristic function of X_i is given as

$$\Phi_{X_i}(t) = \mathbb{E}(e^{itX_i}) = 2\sqrt{-\frac{itC_i}{\sigma_i^2}} K_1\left(2\sqrt{-\frac{itC_i}{\sigma_i^2}}\right), \quad (75)$$

where $K_1(\cdot)$ denotes the modified Bessel function of second kind. Figure 5 shows for different M and N, the absolute values of the correlation matrix of the vector diag $[\mathbf{D}] = [\lambda_1, \lambda_2, \ldots, \lambda_{MN}]^T$. We see from this figure that the entries of diag $[\mathbf{D}]$ are weakly correlated. This is because the off-diagonal values of the covariance matrix are insignificant. The eigenvalues $[\lambda_1, \lambda_2, \ldots, \lambda_{MN}]$ can thus be assumed to be approximately independent. This also implies that the random variables $X_i = |\lambda_i|^{-2}$, for $1 \le i \le n$, are also approximately independent. Figure 1 also validates this assumption wherein the CDF expression of X, derived using this assumption, can be seen to closely match its simulated counterpart. A rigorous proof to show the independence of the eigenvalues is not yet available, and is a crucial direction for future research. The

$$P_{\text{ZF}} = \frac{C_{\mathcal{M}}}{\pi}\int_0^{\frac{\pi}{2}}\int_0^{\infty} \sum_{k=1}^{\log_2\sqrt{\mathcal{M}}} \sum_{i=0}^{(1-2^{-k})\sqrt{\mathcal{M}}-1} \frac{\Psi(i,k)}{\rho\sigma^2} \exp\left(-\frac{(2i+1)^2 3\gamma}{(\mathcal{M}-1)2\sin^2\theta}\right) \exp\left(-\frac{\gamma}{\rho\sigma^2}\right) d\gamma d\theta$$
$$= \frac{C_{\mathcal{M}}}{\pi}\int_0^{\frac{\pi}{2}}\int_0^{\infty} \sum_{k=1}^{\log_2\sqrt{\mathcal{M}}} \sum_{i=0}^{(1-2^{-k})\sqrt{\mathcal{M}}-1} \frac{\Psi(i,k)}{\rho\sigma^2} \exp\left(-\gamma\left(\frac{1}{\rho\sigma^2} + \frac{(2i+1)^2 3\gamma}{(\mathcal{M}-1)2\sin^2\theta}\right)\right) d\gamma d\theta. \quad (69)$$

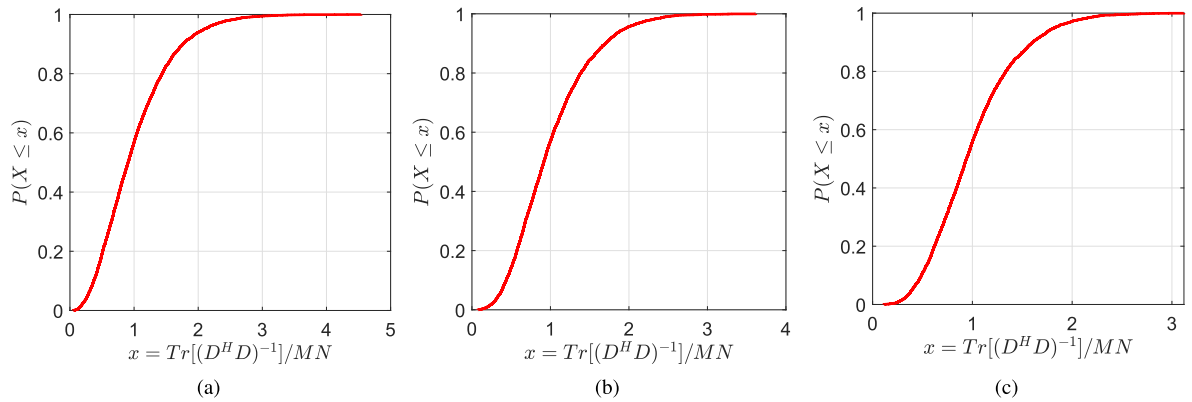

Fig. 6. Empirical CDF of the random variable $\text{Tr}\left[(\mathbf{D}^H\mathbf{D})^{-1}\right]/MN$: (a) $M = N = 8$ and $L_h = 3$; (b) $M = N = 16$ and $L_h = 4$; and (c) $M = N = 32$ and $L_h = 5$.

characteristic function of $X = \sum_{i=1}^{n} C_i X_i$ can be written as:

$$\Phi_X(t) = \prod_{i=1}^{n} \phi_{X_i}(t) = \left\{ 2\sqrt{-\frac{itC_i}{\sigma_i^2}} K_1\left(2\sqrt{-\frac{itC_i}{\sigma_i^2}}\right)\right\}^n. \quad (76)$$

By using the trapezoidal rule with maximum allowable error ε [43], an approximate expression for the CDF of random variable X is obtained using (76) as in (77), as shown at the bottom of the page [43]. The parameter $\Delta > 0$ and K in (78) are respectively chosen as per the conditions given in (32) and (33). The pdf expression in (34) can now be obtained by differentiating (77) w.r.t x.

APPENDIX F

Since the noise vector $\mathbf{v}$ and the error matrix $\mathbf{\Delta D}$ are independent, $\mathbf{G}$ can be obtained as in (78), as shown at the bottom of the page. By substituting $\mathbf{D}^\dagger = (\mathbf{D}^H\mathbf{D})^{-1}\mathbf{D}^H$, the matrix $\mathbf{T}_1$ and $\mathbf{T}_2$ in (78) can be simplified as

$$\mathbf{T}_1 = \sigma_v^2 \mathbf{\Psi}^H(\mathbf{D}^H\mathbf{D})^{-1}\mathbf{\Psi} \text{ and } \mathbf{T}_2 = P_x\sigma_\epsilon^2 \mathbf{\Psi}^H(\mathbf{D}^H\mathbf{D})^{-1}\mathbf{\Psi}.$$

We next simplify the matrix $\mathbf{T}_3$ as follows

$$\mathbf{T}_3 = \sigma_v^2 \mathbf{\Psi}^H(\mathbf{D}^H\mathbf{D})^{-1}\mathbf{D}^H\mathbb{E}[\mathbf{\Delta D}(\mathbf{D}^H\mathbf{D})^{-1}\mathbf{\Delta D}^H] \times \mathbf{D}(\mathbf{D}^H\mathbf{D})^{-1}\mathbf{\Psi}. \quad (79)$$

We know that if elements of a matrix $\mathbf{X} \in \mathbb{C}^{p\times q}$ are i.i.d. with mean zero and variance σ_x^2, then for any Hermitian matrix $\mathbf{R} \in \mathbb{C}^{q\times q}$, the operation $\mathbb{E}[\mathbf{XRX}^H] = \frac{\text{Tr}[\mathbf{R}]}{q}\mathbb{E}[\mathbf{XX}^H]$ [37]. Using this property, we simplify the above matrix $\mathbf{T}_3$ as

$$\begin{aligned}\mathbf{T}_3 &= \sigma_v^2 \text{ Tr}\left[(\mathbf{D}^H\mathbf{D})^{-1}\right]\mathbf{\Psi}^H(\mathbf{D}^H\mathbf{D})^{-1}\mathbf{D}^H\mathbb{E}[\mathbf{\Delta D}\mathbf{\Delta D}^H] \\ &\quad \times \mathbf{D}(\mathbf{D}^H\mathbf{D})^{-1}\mathbf{\Psi} \\ &= \sigma_v^2\sigma_\epsilon^2 \frac{\text{Tr}\left[(\mathbf{D}^H\mathbf{D})^{-1}\right]}{MN}\mathbf{\Psi}^H(\mathbf{D}^H\mathbf{D})^{-1}\mathbf{\Psi}.\end{aligned}$$

Using the $\mathbf{T}_1, \mathbf{T}_2$ and $\mathbf{T}_3$ expressions, the covariance matrix in (78) can be simplified as

$$\mathbf{G} = \sigma_v^2\left[1 + \sigma_\epsilon^2\rho + \sigma_\epsilon^2\frac{\text{Tr}\left[(\mathbf{D}^H\mathbf{D})^{-1}\right]}{MN}\right]\mathbf{\Psi}^H(\mathbf{D}^H\mathbf{D})^{-1}\mathbf{\Psi}. \quad (80)$$

Recall that $\rho = P_x/\sigma_v^2 =$ SNR. At high SNR, the error variance $\sigma_\epsilon^2 \ll 1$. Figure 6 shows the empirical CDF of the random variable $\text{Tr}\left[(\mathbf{D}^H\mathbf{D})^{-1}\right]/MN$ for $M = N = 8, 16, 32$.

We see that the large value of $\text{Tr}\left[(\mathbf{D}^H\mathbf{D})^{-1}\right]/MN$ occur with a small probability. After scaling by σ_ϵ^2, with $\sigma_\epsilon^2 \ll 1$, the third term in the expression in (80) can therefore be ignored. We consequently have $\mathbf{G} = \sigma_v^2\left[1 + \sigma_\epsilon^2\rho\right]\mathbf{\Psi}^H(\mathbf{D}^H\mathbf{D})^{-1}\mathbf{\Psi}$. With the above $\mathbf{G}$ expression, the SINR in (53) for kth symbol with imperfect receive CSI is

$$\hat{\gamma} = \frac{P_x}{\sigma_v^2\left[1 + \sigma_\epsilon^2\rho\right]\left[\mathbf{\Psi}^H(\mathbf{D}^H\mathbf{D})^{-1}\mathbf{\Psi}\right]_{k,k}} = \frac{\rho MN}{(1+\sigma_\epsilon^2\rho)\sum_{i=1}^{MN}\frac{1}{|\lambda_i|^2}} = \frac{1}{1+\sigma_\epsilon^2\rho}\gamma. \quad (81)$$

Here $\gamma = \rho MN/\sum_{i=1}^{MN}\frac{1}{|\lambda_i|^2}$ is the SINR with perfect receive CSI, which is derived in (12).

$$\Pr(X \leq x) \approx \frac{1}{2} - \frac{1}{\pi}\sum_{k=0}^{K}\Im\left[\frac{\exp\left\{-i\left(k+\frac{1}{2}\right)\Delta x\right\}\Phi_X\left\{\left(k+\frac{1}{2}\right)\Delta\right\}}{\left(k+\frac{1}{2}\right)}\right]. \quad (77)$$

$$\begin{aligned}\mathbf{G} &= \mathbb{E}[\mathbf{\Psi}^H\mathbf{D}^\dagger\mathbf{\Psi}\mathbf{v}\mathbf{v}^H\mathbf{\Psi}^H\mathbf{D}^{\dagger^H}\mathbf{\Psi}] + \mathbb{E}[\mathbf{\Psi}^H\mathbf{D}^\dagger\mathbf{\Delta D}\mathbf{\Psi}\mathbf{x}\mathbf{x}^H\mathbf{\Psi}^H\mathbf{\Delta D}^H\mathbf{D}^{\dagger^H}\mathbf{\Psi}] + \mathbb{E}[\mathbf{\Psi}^H\mathbf{D}^\dagger\mathbf{\Delta D}\mathbf{D}^\dagger\mathbf{\Psi}\mathbf{v}\mathbf{v}^H\mathbf{\Psi}^H\mathbf{D}^{\dagger^H}\mathbf{\Delta D}^H\mathbf{D}^{\dagger^H}\mathbf{\Psi}] \\ &= \underbrace{\sigma_v^2[\mathbf{\Psi}^H\mathbf{D}^\dagger\mathbf{D}^{\dagger^H}\mathbf{\Psi}]}_{\mathbf{T}_1} + \underbrace{P_x\sigma_\epsilon^2[\mathbf{\Psi}^H\mathbf{D}^\dagger\mathbf{D}^{\dagger^H}\mathbf{\Psi}]}_{\mathbf{T}_2} + \underbrace{\sigma_v^2\mathbb{E}[\mathbf{\Psi}^H\mathbf{D}^\dagger\mathbf{\Delta D}\mathbf{D}^\dagger\mathbf{D}^{\dagger^H}\mathbf{\Delta D}^H\mathbf{D}^{\dagger^H}\mathbf{\Psi}]}_{\mathbf{T}_3}. \quad (78)\end{aligned}$$

REFERENCES

[1] A. Goldsmith, *Wireless Communications* Cambridge, U.K.: Cambridge Univ. Press, 2005.

[2] T. Wang, J. G. Proakis, E. Masry, and J. R. Zeidler, "Performance degradation of OFDM systems due to Doppler spreading," *IEEE Trans. Wireless Commun.*, vol. 5, no. 6, pp. 1422–1432, Jun. 2006.

[3] S. K. Mohammed, "Derivation of OTFS modulation from first principles," *IEEE Trans. Veh. Technol.*, vol. 70, no. 8, pp. 7619–7636, Aug. 2021.

[4] V. Khammammetti and S. K. Mohammed, "OTFS-based multiple-access in high Doppler and delay spread wireless channels," *IEEE Wireless Commun. Lett.*, vol. 8, no. 2, pp. 528–531, Apr. 2019.

[5] K. Deka, A. Thomas, and S. Sharma, "OTFS-SCMA: A code-domain NOMA approach for orthogonal time frequency space modulation," *IEEE Trans. Commun.*, vol. 69, no. 8, pp. 5043–5058, Aug. 2021.

[6] H. Qu, G. Liu, L. Zhang, M. A. Imran, and S. Wen, "Low-dimensional subspace estimation of continuous-Doppler-spread channel in OTFS systems," *IEEE Trans. Commun.*, vol. 69, no. 7, pp. 4717–4731, Jul. 2021.

[7] Y. Ge, Q. Deng, P. C. Ching, and Z. Ding, "Receiver design for OTFS with a fractionally spaced sampling approach," *IEEE Trans. Wireless Commun.*, vol. 20, no. 7, pp. 4072–4086, Jul. 2021.

[8] L. Gaudio, M. Kobayashi, G. Caire, and G. Colavolpe, "On the effectiveness of OTFS for joint radar parameter estimation and communication," *IEEE Trans. Wireless Commun.*, vol. 19, no. 9, pp. 5951–5965, Sep. 2020.

[9] S. Tiwari, S. S. Das, and V. Rangamgari, "Low complexity LMMSE receiver for OTFS," *IEEE Commun. Lett.*, vol. 23, no. 12, pp. 2205–2209, Dec. 2019.

[10] R. Hadani *et al.*, "Orthogonal time frequency space modulation," in *Proc. IEEE WCNC*, San Francisco, CA, USA, Mar. 2017, pp. 1–6.

[11] G. D. Surabhi and A. Chockalingam, "Low-complexity linear equalization for OTFS modulation," *IEEE Commun. Lett.*, vol. 24, no. 2, pp. 330–334, Feb. 2020.

[12] Z. Wei *et al.*, "Orthogonal time-frequency space modulation: A promising next-generation waveform," *IEEE Wireless Commun.*, vol. 28, no. 4, pp. 136–144, Aug. 2021.

[13] G. D. Surabhi, R. M. Augustine, and A. Chockalingam, "On the diversity of uncoded OTFS modulation in doubly-dispersive channels," *IEEE Trans. Wireless Commun.*, vol. 18, no. 6, pp. 3049–3063, Jun. 2019.

[14] P. Raviteja, K. T. Phan, Y. Hong, and E. Viterbo, "Interference cancellation and iterative detection for orthogonal time frequency space modulation," *IEEE Trans. Wireless Commun.*, vol. 17, no. 10, pp. 6501–6515, Oct. 2018.

[15] M. K. Ramachandran and A. Chockalingam, "MIMO-OTFS in high-Doppler fading channels: Signal detection and channel estimation," in *Proc. IEEE Global Commun. Conf. (GLOBECOM)*, Abu Dhabi, United Arab Emirates, Dec. 2018, pp. 206–212.

[16] G. D. Surabhi, M. K. Ramachandran, and A. Chockalingam, "OTFS modulation with phase noise in mmWave communications," in *Proc. IEEE 89th Veh. Technol. Conf. (VTC-Spring)*, Kuala Lumpur, Malaysia, Apr. 2019, pp. 1–5.

[17] K. R. Murali and A. Chockalingam, "On OTFS modulation for high-Doppler fading channels," in *Proc. Inf. Theory Appl. Workshop (ITA)*, San Diego, CA, USA, Feb. 2018, pp. 1–10.

[18] G. D. Surabhi and A. Chockalingam, "Low-complexity linear equalization for 2×2 MIMO-OTFS signals," in *Proc. IEEE 21st Int. Workshop Signal Process. Adv. Wireless Commun. (SPAWC)*, Atlanta, GA, USA, May 2020, pp. 1–5.

[19] W. Yuan, Z. Wei, J. Yuan, and D. W. K. Ng, "A simple variational Bayes detector for orthogonal time frequency space (OTFS) modulation," *IEEE Trans. Veh. Technol.*, vol. 69, no. 7, pp. 7976–7980, Jul. 2020.

[20] P. Singh, A. Gupta, H. B. Mishra, and R. Budhiraja, "Low-complexity ZF/MMSE receivers for MIMO-OTFS systems with imperfect CSI," 2020, *arXiv:2010.04057*.

[21] J. Feng, H. Q. Ngo, M. F. Flanagan, and M. Matthaiou, "Performance analysis of OTFS-based uplink massive MIMO with ZF receivers," in *Proc. IEEE ICC Workshops*, Montreal, QC, Canada, Jun. 2021, pp. 1–7.

[22] P. Singh, H. B. Mishra, and R. Budhiraja, "Low-complexity linear MIMO-OTFS receivers," in *Proc. IEEE Int. Conf. Commun. Workshops (ICC Workshops)*, Montreal, QC, Canada, Jun. 2021, pp. 1–6.

[23] T. L. Marzetta, *Fundamentals Massive MIMO*. Cambridge, U.K.: Cambridge Univ. Press, 2016.

[24] H. Q. Ngo, E. G. Larsson, and T. L. Marzetta, "Energy and spectral efficiency of very large multiuser MIMO systems," *IEEE Trans. Commun.*, vol. 61, no. 4, pp. 1436–1449, Apr. 2013.

[25] Z. Wang, X. Chen, and X. Ning, "BER analysis of integrated WFRFT-OTFS waveform framework over static multipath channels," *IEEE Commun. Lett.*, vol. 25, no. 3, pp. 754–758, Mar. 2021.

[26] M. Rupp, S. Schwarz, and M. Taranetz, *The Vienna LTE-Advanced Simulators*. Singapore: Springer, 2016.

[27] A. Fish, S. Gurevich, R. Hadani, A. M. Sayeed, and O. Schwartz, "Delay-Doppler channel estimation in almost linear complexity," *IEEE Trans. Inf. Theory*, vol. 59, no. 11, pp. 7632–7644, Nov. 2013.

[28] Z. Ding, R. Schober, P. Fan, and H. Vincent Poor, "OTFS-NOMA: An efficient approach for exploiting heterogenous user mobility profiles," *IEEE Trans. Commun.*, vol. 67, no. 11, pp. 7950–7965, Nov. 2019.

[29] P. Raviteja, E. Viterbo, and Y. Hong, "OTFS performance on static multipath channels," *IEEE Wireless Commun. Lett.*, vol. 8, no. 3, pp. 745–748, Jun. 2019.

[30] C. Wang, E. K. S. Au, R. D. Murch, W. H. Mow, R. S. Cheng, and V. Lau, "On the performance of the MIMO zero-forcing receiver in the presence of channel estimation error," *IEEE Trans. Wireless Commun.*, vol. 6, no. 3, pp. 805–810, Mar. 2007.

[31] E. K. S. Au *et al.*, "Error probability for MIMO zero-forcing receiver with adaptive power allocation in the presence of imperfect channel state information," *IEEE Trans. Wireless Commun.*, vol. 6, no. 4, pp. 1523–1529, Apr. 2007.

[32] M. Ramachandran, G. Surabhi, and A. Chockalingam, "OTFS: A new modulation scheme for high-mobility use cases," *J. Indian Inst. Sci.*, vol. 100, no. 2, pp. 315–336, 2020.

[33] P. Singh, H. B. Mishra, A. K. Jagannatham, K. Vasudevan, and L. Hanzo, "Uplink sum-rate and power scaling laws for multi-user massive MIMO-FBMC systems," *IEEE Trans. Commun.*, vol. 68, no. 1, pp. 161–176, Jan. 2020.

[34] D. A. Gore, R. W. Heath, Jr., and A. J. Paulraj, "Transmit selection in spatial multiplexing systems," *IEEE Commun. Lett.*, vol. 6, no. 11, pp. 491–493, Nov. 2002.

[35] M. Kiessling and J. Speidel, "Analytical performance of MIMO zero-forcing receivers in correlated Rayleigh fading environments," in *Proc. SPAWC*, Rome, Italy, Jun. 2003, pp. 383–387.

[36] K. Cho and D. Yoon, "On the general BER expression of one-and two-dimensional amplitude modulations," *IEEE Trans. Commun.*, vol. 50, no. 7, pp. 1074–1080, Jul. 2002.

[37] P. Singh, H. B. Mishra, A. K. Jagannatham, and K. Vasudevan, "Semi-blind, training, and data-aided channel estimation schemes for MIMO-FBMC-OQAM systems," *IEEE Trans. Signal Process.*, vol. 67, no. 18, pp. 4668–4682, Sep. 2019.

[38] A. Papoulis and H. Saunders, *Probability, Random Variables and Stochastic Processes*. New York, NY, USA: McGraw-Hill, 2002.

[39] N. L. Johnson, S. Kotz, and N. Balakrishnan, *Continuous Univariate Distributions*, vol. 2. Hoboken, NJ, USA: Wiley, 1995.

[40] S. Nadarajah and S. Kotz, "On the product and ratio of Gamma and Beta random variables," *Allgemeines Statist. Arch.*, vol. 89, no. 4, pp. 435–449, 2005.

[41] M. Geller and E. W. Ng, "A table of integrals of the exponential integral," *J. Res. Nat. Bur. Standards*, vol. 71, pp. 1–20, Jan. 1969.

[42] C. Tellambura, M. Soysa, and D. Senaratne, "Performance analysis of wireless systems from the MGF of the reciprocal of the signal-to-noise ratio," *IEEE Commun. Lett.*, vol. 15, no. 1, pp. 55–57, Jan. 2011.

[43] V. Witkovský, "Computing the distribution of a linear combination of inverted gamma variables," *Kybernetika*, vol. 37, no. 1, pp. 79–90, 2001.

[44] E. W. Ng and M. Geller, "A table of integrals of the error functions," *J. Res. Nat. Bur. Standards-B. Math. Sci.*, vol. 73, no. 1, pp. 1–14, 1969.

[45] Y. L. Luke, *Special Functions and Their Approximations*. New York, NY, USA: Academic, 1969.

[46] P. Raviteja, K. T. Phan, and Y. Hong, "Embedded pilot-aided channel estimation for OTFS in delay–Doppler channels," *IEEE Trans. Veh. Technol.*, vol. 68, no. 5, pp. 4906–4917, May 2019.

[47] H. B. Mishra, P. Singh, A. K. Prasad, and R. Budhiraja, "OTFS channel estimation and data detection designs with superimposed pilots," *IEEE Trans. Wireless Commun.*, early access, Sep. 15, 2021, doi: 10.1109/TWC.2021.3110659.

[48] *3rd Generation Partnership Project; Technical Specification Group Radio Access Network: Evolved Universal Terrestrial Radio Access (E-UTRA): User Equipment (UE) Conformance Specification Radio Transmission and Reception*, UEUE Conformance Specification; Radio Transmission and Reception, France, 2011.

[49] A. Chockalingam and B. S. Rajan, *Large MIMO Systems*. Cambridge, U.K.: Cambridge Univ. Press, 2014.

[50] I. Kra and S. R. Simanca, "On circulant matrices," *Notices Amer. Math. Soc.*, vol. 59, no. 3, pp. 368–377, Mar. 2012.

[51] Y.-P. Lin, S.-M. Phoong, and P. Vaidyanathan, *Filter Bank Transceivers for OFDM and DMT Systems*. Cambridge, U.K.: Cambridge Univ. Press, 2010.
[52] J. W. Craig, "A new, simple and exact result for calculating the probability of error for two-dimensional signal constellations," in *Proc. IEEE Military Commun. Conf.*, vol. 2, Nov. 1991, pp. 571–575.
[53] M. K. Simon and M. Alouini, *Digital Communication Over Fading Channels*. Hoboken, NJ, USA: Wiley, 2004.

Prem Singh received the M.Tech. and Ph.D. degrees in electrical engineering from the Indian Institute of Technology Kanpur, India, in 2011 and 2020, respectively. He worked as a Project Executive Officer on the Indigenous 5G TestBed Project, where he developed hardware and software algorithms for an end-to-end 3GPP compliant 5G-NR testbed. Since July 2021, he has been working as an Assistant Professor with the International Institute of Information Technology (IIIT) Bangalore, India. His research interests lie in the area of parameter estimation and transceiver design for 5G and next-generation wireless technologies including filter bank multicarrier (FBMC), orthogonal time–frequency space (OTFS), massive MIMO, and millimeter-wave. His interests also lie in the area of designing practical 4G/5G wireless systems using 3GPP standards. His Ph.D. thesis got selected for the final round (top two) for the Indian National Academy of Engineering (INAE) Innovative Student Project Award 2021 at the doctoral level. He received the Best Ph.D. Thesis Award at the 4th IEEE International Conference on Information and Communication Technology (CICT) 2020 organized by IIITDM Kancheepuram, India.

Khushboo Yadav received the M.Tech. degree in electrical engineering, with specialization in signal processing, communication, and networks, from IIT Kanpur. Currently, she is working as a Modem System Engineer at Qualcomm. Her area of interests constitute wireless communication and signal processing.

Himanshu B. Mishra (Member, IEEE) received the M.Tech. degree in electronics and communication engineering from the National Institute of Technology Rourkela, Rourkela, India, in 2012, and the Ph.D. degree in electrical engineering from the Indian Institute of Technology Kanpur, Kanpur, India, in 2016. He is currently working as an Assistant Professor with the Electronics Engineering Department, Indian Institute of Technology (Indian School of Mines) Dhanbad, India. His current research interests include the area of signal processing, next generation of wireless communication systems, estimation, and detection theory. He received the Best M.Tech. Award in the communication and signal processing domain.

Rohit Budhiraja received the M.S. degree in electrical engineering and the Ph.D. degree from IIT Madras in 2004 and 2015, respectively. From 2004 to 2011, he worked for two start-ups where he designed both hardware and software algorithms, from scratch, for physical layer processing of WiMAX- and LTE-based cellular systems. He is currently an Assistant Professor with IIT Kanpur, where he is also leading an effort to design a 5G research testbed. His current research interests include design of energy-efficient transceiver algorithms for 5G massive MIMO and full-duplex systems, robust precoder design for wireless relaying, machine learning methods for channel estimation in mm-wave systems, and spatial modulation systems design. His paper was shortlisted as one of the finalists for the Best Student Paper Awards at the IEEE International Conference on Signal Processing and Communications, Bengaluru, India, in 2014. He also received the IIT Madras Research Award for the quality and quantity of research work done in his Ph.D. degree, the Early Career Research Award, and the Teaching Excellence Certificate at IIT Kanpur.